# Supplementary Information for Three-dimensional Printing of High-Performance Hydrogel Bioelectronic Implants

Yuan Yao[1,2,†,*], Jianhua Luo[3,4,5,†], Yue Hui[6,†], Jiahua Lyu[7], Yubin Ke[8], Wenhao Shen[1,2], Yuchen Xu[9], Yetian Yu[2], Hongcai Chen[10], Mohamad Sawan[9], Liang Tao[1,3,4,5,*], Nanjia Zhou[1,2,11,*]

[1]Research Center for Industries of the Future, Westlake University, Hangzhou, 310030, China

[2]Key Laboratory of 3D Micro/Nano Fabrication and Characterization of Zhejiang Province, School of Engineering, Westlake University, Hangzhou, 310024, Zhejiang Province, China.

[3]Zhejiang Key Laboratory of Multi-Omics in Infection and Immunity, Westlake Laboratory of Life Sciences and Biomedicine, Hangzhou, 310024, China

[4]Affiliated Hangzhou First People's Hospital, School of Medicine, Westlake University, Hangzhou, 310030, China

[5]School of Life Sciences, Westlake University, Hangzhou, 310030, China

[6]School of Chemical Engineering and Advanced Materials, the University of Adelaide, Adelaide, 5005, South Australia, Australia.

[7]College of Advanced Interdisciplinary Studies, National University of Defense Technology, Changsha, 410000, China

[8]Spallation Neutron Source Science Center, Institute of High Energy Physics, Chinese Academy of Sciences, Dongguan, 523803, China

[9]CenBRAIN Neurotech Center of Excellence, School of Engineering, Westlake University, Hangzhou, 310030, China

[10]School of Automation, Southeast University, Nanjing 210096, China

[11]Enovate 3D (Hangzhou) Technology Development CO., LTD. 2-606, No. 6 Lianhui Street, Xixing Sub-district, Binjiang District, Hangzhou, 310051, China

†These authors contributed equally to this work.

*To whom correspondence should be addressed; Email: yaoyuan@westlake.edu.cn (Y.Y), taoliang@westlake.edu.cn (L.T.), zhounanjia@westlake.edu.cn (N.Z.)

## Materials and Methods

### Materials

Hydroxyethyl acrylate (HEA), ethyl acrylate (EA), hydroxyethyl methacrylate (HEMA), 2-methoxyethyl acrylate (MEA), acrylic acid (AA), acrylamide (AM), α-ketoglutaric acid (α-KA), Poly(ethylene oxide) (PEO, 1000 kDa), ammonium persulfate (APS), *N,N′*-methylenebisacrylamide (MBAA) and ethylene glycol dimethyacrylate (EGMDA) were purchased from Sigma-Aldrich. 3-(Trimethoxysilyl) propyl methacrylate (TMSPMA) was purchased from TCL. Hexane and D-(+)-Gluconic acid δ-lactone (GDL) were purchased from Rhawn. Ethylenediaminetetraacetic acid (EDTA) was purchased from Macklin. Calcium chloride ($CaCl_2$), sodium hydroxide and acetic acid was purchased from General-Reagent. Defoaming agent XS-101 was obtained from Foshan Nanhai Taiyang Electroplating and Anticorrosion Materials Co., Ltd. Ag flakes (5 μm) was purchased from Shanghai Yao Tian Nano Material. The LED (part no. ORH-B37A) was purchased from Orient. The surface mount Schottky barrier rectifier (marketing code: S14) was purchased from Oubeidun.

### Purification of HEA monomer

The HEA monomer was purified to remove the residual EGDMA analogues. In detail, 20 g of HEA monomer was dissolved in 80 mL deionized water and then transferred into a separating funnel. 100 mL of n-hexane was added into funnel and mixed with HEA solution. The mixture was allowed to settle for phase-separation. The upper n-hexane part was then removed. This process was repeated for six times. Thereafter, the purified HEA solution was transferred into a rotary evaporator (IKA RV 10) for completely removal of water. The average yield was around 95 to 97%.

### Preparation of HEA/EA monomer micelle solutions

The HEA/EA monomer micelle solution with a water-to-monomer ratio of 4.0 was prepared by dissolving 0.0187 M of purified HEA, 0.00934 M of EA in 2 g of deionized water. The HEA/EA monomer micelle solution with a water-to-monomer ratio of 3.0 was prepared by dissolving 0.024 M of purified HEA, 0.012 M of EA in 2 g of deionized water. The HEA/EA monomer micelle solution with a water-to-monomer ratio of 2.5 was prepared by dissolving 0.0293 M of purified HEA, 0.0147 M of EA in 2 g of deionized water. The HEA/EA monomer micelle solution with a water-to-monomer ratio of 2.1 was prepared by dissolving 0.0347 M of purified HEA, 0.0173 M of EA in 2 g of deionized water. The mixtures were mixed thoroughly to form homogeneous micelle solutions.

Synthesis of PHEA-PEA anti-swelling hydrogels (AS-hydrogels)

The appropriate amount of α-KA (1 wt% of monomers) was added into the abovementioned HEA/EA micelle solutions. After α-KA was fully dissolved, the mixture was transferred into a custom-made PTFE mold (50 mm × 40 mm × 2 mm). A glass coverslip was used to cover the PTFE mold. Then, a 365 nm UV lamp was used to cure the micelle solution, the power density was controlled at ~ 2.5 mW/cm$^2$. The curing process was allowed to last for 1 hours. The cured PHEA-PEA hydrogels was then dialyzed in water for at least 24 hours to remove the residual monomers and α-KA. The final monomer conversion of each batch was determined gravimetrically, the average monomer conversion was above 90% (even for those opaque PHEA-PEA AS-hydrogels).

Determination of swelling factors of hydrogels

All the hydrogel samples were cured in a custom-made round PTFE mold with a diameter of 20 mm and a height of 2 mm. The initial weight of the cured hydrogel was recorded as $M_0$. The hydrogel was then transferred to a beak with 50 mL of water and allowed to swell to equilibrium for at least 2 days. The weight after swollen was recorded as $M_1$. The swelling factor ($Q$) was calculated as

$$Q = \frac{M_1 - M_0}{M_0} \times 100\% \quad (1)$$

Preparation of HEMA monomer micelle solutions

The HEMA monomer micelle solution with a water-to-monomer ratio of 7.0 was prepared by dissolving 0.016 M of HEMA in 2 g of deionized water. The HEMA monomer micelle solution with a water-to-monomer ratio of 5.6 was prepared by dissolving 0.02 M of HEMA in 2 g of deionized water. The HEMA monomer micelle solution with a water-to-monomer ratio of 4.6 was prepared by dissolving 0.024 M of HEMA in 2 g of deionized water. The HEMA monomer micelle solution with a water-to-monomer ratio of 4.0 was prepared by dissolving 0.028 M of HEMA in 2 g of deionized water. The mixtures were mixed thoroughly to form homogeneous micelle solution.

Synthesis of PHEMA AS-hydrogels

The appropriate amount of α-KA (1 wt% of monomers) was added into the abovementioned HEMA micelle solutions. After α-KA was fully dissolved, the mixture was transferred into a custom-made PTFE mold (50 mm × 40 mm × 2 mm). A glass slice was used to cover the PTFE mold. Then, a 365 nm UV lamp was used to cure the micelle solution, the power density was controlled at ~ 2.5 mW/cm$^2$. The curing process was allowed to last for 2 hours. The cured PHEMA hydrogels was then dialyzed in water for at least 24 hours to remove

the residual monomers and α-KA. The final monomer conversion of each batch was determined gravimetrically, the average monomer conversion was above 93.2%.

Preparation of MEA/HEA monomer micelle solutions

The MEA/EA monomer micelle solution with a water-to-monomer ratio of 6.1 was prepared by dissolving 0.012 M of MEA, 0.006 M of purified HEA in 2 g of deionized water. The MEA/HEA monomer micelle solution with a water-to-monomer ratio of 4.1 was prepared by dissolving 0.018 M of MEA, 0.009 M of purified HEA in 2 g of deionized water. The MEA/HEA monomer micelle solution with a water-to-monomer ratio of 3.1 was prepared by dissolving 0.024 M of MEA, 0.012 M of purified HEA in 2 g of deionized water. The MEA/HEA monomer micelle solution with a water-to-monomer ratio of 2.6 was prepared by dissolving 0.028 M of MEA, 0.014 M of purified HEA in 2 g of deionized water. The mixtures were mixed thoroughly to form homogeneous micelle solution.

Synthesis of PMEA-PHEA AS-hydrogels

The appropriate amount of α-KA (1 wt% of monomers) was added into the abovementioned MEA/HEA micelle solutions. After α-KA was fully dissolved, the mixture was transferred into a custom-made PTFE mold (50 mm × 40 mm × 2 mm). A glass slice was used to cover the PTFE mold. Then, a 365 nm UV lamp was used to cure the micelle solution, the power density was controlled at ~ 2.5 $mW/cm^2$. The curing process was allowed to last for 1 hours. The cured PMEA-PHEA hydrogels was then dialyzed in water for at least 24 hours to remove the residual monomers and α-KA. The final monomer conversion of each batch was determined gravimetrically, the average monomer conversion was above 96.2%.

Preparation of AA/AM/EA monomer micelle solutions

The AA/AM/EA monomer micelle solution with a water-to-monomer ratio of 3.1 was prepared by dissolving 0.018 M of AA, 0.009 M of AM and 0.009 M of EA in 2 g of deionized water. The AA/AM/EA monomer micelle solution with a water-to-monomer ratio of 2.5 was prepared by dissolving 0.022 M of AA, 0.011 M of AM and 0.011 M of EA in 2 g of deionized water. The AA/AM/EA monomer micelle solution with a water-to-monomer ratio of 2.1 was prepared by dissolving 0.026 M of AA, 0.013 M of AM and 0.013 M of EA in 2 g of deionized water. The AA/AM/EA monomer micelle solution with a water-to-monomer ratio of 1.9 was prepared by dissolving 0.03 M of AA, 0.015 M of AM and 0.015 M of EA in 2 g of deionized water. The mixtures were sonicated at room temperature for at least 20 minutes to form homogeneous micelle solutions.

Synthesis of PAA-PAM-PEA AS-hydrogels

The appropriate amount of α-KA (1 wt% of monomers) was added into the abovementioned AA/AM/EA micelle solutions. After α-KA was fully dissolved, the mixture was transferred into a custom-made PTFE mold (50 mm × 40 mm × 2 mm). A glass slice was used to cover the PTFE mold. Then, a 365 nm UV lamp was used to cure the micelle solution, the power density was controlled at ~ 2.5 mW/cm$^2$. The curing process was allowed to last for 1 hours. The cured PAA-PAM-PEA hydrogels was then dialyzed in water for at least 24 hours to remove the residual monomers and α-KA. The final monomer conversion of each batch was determined gravimetrically, the average monomer conversion was above 90.2%.

The small angle neutron scattering (SANS) measurements

SANS measurements were performed on the Small-angle Neutron Diffractometer at China Spallation Neutron Source (CSNS). The incident neutrons with wavelength of 1.2–9.8 Å were defined by a double-disc bandwidth chopper, which was collimated to the sample by a pair of apertures. The experiment used the sample to detector distance of 4 m and a sample aperture of 6 mm in diameter. The two dimensional 3He tubes array detector allows to cover a wide Q range from 0.005 Å$^{-1}$ to 0.70 Å$^{-1}$. We collected approximate 60 min scattering information for each sample, including the empty sample holder, sample cell and the solvent. The scattering data were set to absolute unit after normalization, transmission correction and standard sample calibration.

The aqueous atomic force microscopy imaging of AS-hydrogels

2 g of TMSPMA was dissolved in 98 mL of deionized water, followed by the addition of 10 μL acetic acid. The mixture was stirred at room temperature until the oil droplets completely disappeared. Meanwhile, a custom-made spherical borosilicate glass (D=35 mm, H=1mm) was clean by ethanol, followed by a UV plasma treatment for 5 min. The treatment glass was immersed in the hydrolyzed TMSPMA solution for 2 hours and cleaned by washing with ethanol and deionized water repeatably. The treated glass was further air dried at stored at 4 ºC before use. The treated glass was assembled with a custom-made square PTFE mold with a spherical piercing (D=15 mm, H=2 mm) on top. The assembled mold was clamped by four stainless steel clamps. The monomer micelle solution was transferred into the assembled mold, a glass coverslip was used to cover the mold during curing. Thereafter, the monomer micelle solution was *in-situ* cured inside the mold by a 365 UV lamp at a power density of ~ 2.5 mW/cm$^2$. After curing, a spherical AS-hydrogel was obtained which was covalently attached to the treated glass. Next, the AS-hydrogel/glass was dialyzed in deionized water for at least 2 days. The AS-hydrogel/glass was assembled with the liquid imaging module, followed by adding certain amount of deionized water. The aqueous atomic force images were then acquired by an AFM (Jupiter XR, Oxford Instruments).

Mechanical test for AS-hydrogels

The monomer micelle solutions were fully cured in a custom-made dumbbell-shaped PTFE mold (ISO 37-3) to form AS-hydrogels. All the AS-hydrogel specimens were swollen to equilibrium in water for at least 2 days. Before test, the all the AS-hydrogel specimens were covered by a layer of silicone oil for prevention of the dehydration during the test. For tensile tests, the AS-hydrogel specimens were loaded to the Instron 34SC-1 equipped with a 1KN force sensor and a pneumatic grip control system. The loading rate was set to 0.025 $s^{-1}$. The Young's modulus was measured from the initial slope of stress-strain curve.

Animal experiments

All the animal procedures reported herein were approved by the Institutional Animal Care and Use Committee at Westlake University (IACUC Protocol #22-041-TL, #24-111-TL). Balb/c mice and SD rats (female, 6-8 weeks) were purchased from Laboratory Animal Resources Center at Westlake University (Hangzhou, China). Animal were housed with food and water without limitation and monitored under the care of full-time staff. For the surgical procedures, animals were anesthetized via either intraperitonea injection of 1% sodium pentobarbital, or anaesthetized using 3% inhaled isoflurane and maintained with a nose cone and 1-2% isoflurane in $O_2$. Animal was fixed in the 37℃-operating table, sterile eye ointment was applied to protect corneal. The surgical sites of the animals were shaved and given analgesics subcutaneously, the exposed area was disinfected with iodine. After surgical, the wound was sutured and disinfected, animals were allowed to recover in a 37°C thermostatic environment. After experiments are done, all animals were euthanized with $CO_2$ gas.

Subcutaneous implantation experiment

A 1cm incision was made on the back, and the skin was bluntly separated. The "mock device", either hydrogel or silicone, was implanted under the skin of the mouse. In the sham operation group, only blunt separation was performed. Thereafter, The mouse was allowed to recover at 37 degrees. After 2 or 8-week implantation, skin segments were extracted, fixed, paraffin-embedded, sectioned and subjected to either H&E staining for histological score analysis or mIHC analysis.

H&E Staining, Histopathological Analysis, and Multiplexed immunohistochemistry(mIHC)

After Skin specimens were fixed in formalin for 12 h before being dehydrated by using an alcohol gradient, cleared with xylene then embedded in paraffin. Paraffin blocks were cut into 5 μm sections and stained with hematoxylin and eosin. The H&E staining sections were scored blinded by pathologist based on inflammatory cell infiltration on a scale of 0 to 3 (mild to severe). The mIHC protocol with primary antibodies sequentially and paired with TSA 6-color kit (abs50038-100T, Absinbio). Then by staining with DAPI (abs47047616, Absinbio). For example, deparaffinized slides were incubated with anti- CD201 antibody (#ab302911, Abcam), for 1 hour and then treated with anti-rabbit/mouse horseradish peroxidase-conjugated (HRP) secondary antibody (abs50015-02, Absinbio) for 10 minutes. Then labelling was developed for a strictly observed 10 minutes, using TSA 650 per manufacturer's direction. Slides were washed in TBST buffer and then transferred to preheated citrate solution (90°C) before being heat-treated using a microwave set at 20% of maximum power for 15 minutes. Slides were cooled in the same solution to room temperature. Between all steps, the slides were washed with Tris-buffer. The same process was repeated for the following antibodies/fluorescent dyes, in order: anti-α-SMA/ TSA 520, anti-Vimentin/ TSA 570, anti-DCN/ TSA 660S and anti-COL1A1/ TSA 700. Each slide was then treated with 2 drops of DAPI, washed in distilled water, and manually cover slipped. Slides were air dried and take pictures with Pannoramic MIDI II (3DHISTECH). Images was analyzed using Indica Halo software.

RNA-seq analysis

After implantation or sham operation and freshly collected skin tissue (100 -150mg) were flash-frozen and stored in liquid nitrogen. Following RNA purification, reverse transcription, and library construction, sequencing was performed at Shanghai Majorbio Bio-pharm Biotechnology Co., Ltd. (Shanghai, China). Conducting differential expression analysis involves assessing quantitative expression results to identify genetic variations between groups. Differential expression is determined by evaluating the gain of differentially expressed genes between each group using the variance analysis software EdgeR. The applied threshold criteria for significance are set as $|\log2FC| \geq 1$ and $P$ value $< 0.05$.

Statistical analysis

All tests were two-tailed, and a $P$ value of $< 0.05$ was considered statistically significant. Data were plotted and analyzed using GraphPad Prism (version 9.0) and represented as mean ± SEM. Detailed statistical information, including the tests used and the exact value of n, is provided in the figure legends. Here, n denotes the exact number of animals for *in vivo* studies and the exact number of biological repeats for in *vitro* studies.

Preparation of curable AS-hydrogel based support matrices

The MEA/HEA monomer micelle solution with a water-to-monomer molar ratio of 2.6 was first prepared by dissolving 0.056 M of MEA, 0.028 M of purified HEA in 4 g of deionized water. The appropriate amount of α-KA (1 wt% of monomers) was added to monomer micelle solution and mixed thoroughly. The solution was then UV cured in a custom-made PTFE mold to form PMEA-PHEA AS-hydrogel. The AS-hydrogel was then dialyzed in water for 2 days for removing the residual monomers and initiators. Thereafter the purified AS-hydrogel was cut into pieces and transferred into a 50 mL stainless steel ball mill tank equipped with a stainless steel ball-milling ball with a diameter of 20 mm. Both the AS-hydrogels and ball mill tank were cooled by liquid nitrogen for at least 10 minutes. Then a freeze ball-milling process was performed by a cryogenic grinder (JXFSTPRP-CLN, Jingxin) at 60 Hz for a duration of 45 seconds. The pulverized AS-hydrogel particles were immediately transferred into a 100 mL container and allowed to swell in a MEA/HEA monomer micelle solution (water-to-monomer molar ratio of 2.6) with a varying particle to solution weight ratios at 1: 4.5, 1:5.5, 1:6.5 and 1:7.5. The mixture was mixed using a planetary mixer (FlackTek SpeedMixer DAC 1200) at 2000 rpm for 1 minute. Next, the mixture was settled for 3 days allowing the pulverized AS-hydrogel particles to be fully swollen to form a yield-stress like supporting matrix. Thereafter, the matrix underwent a freeze-ball milling process two additional times. The ball-milled matrices were subsequently filtered by using a 75 μm nylon membrane, followed by adding appropriate amount of α-KA (1 wt% of matrix) and APS (0.3% wt of matrix). The resulted matrix was mixed and degassed using a planetary mixer (ARE-310, Thinky) and stored at 4 ºC before use (Supplementary Fig. 23).

Preparation of hydrogel matrix for conductive hydrogel ink

The PMEA-PHEA AS-hydrogel was prepared according to the abovementioned approaches and dialyzed in water for 1 days for removing the residual monomers and initiators. The swollen AS-hydrogel was then pulverized into micron-sized particles using a freeze ball milling method as described before. The pulverized AS-hydrogel particles were allowed to swell in a MEA/HEA monomer micelle solution (water-to-monomer molar ratio of 2.6) with a particle to solution weight ratios at 1:9. The mixture was mixed using a SpeedMixer at 2000 rpm for 1 minute, and allowed to settle for 3 days, forming homogenous hydrogel matrix. The hydrogel matrix was further freeze ball milled for two additional times, and filtered with a 10 μm syringe filter. The filtered hydrogel matrix was stored at 4 ºC before use.

Preparation of printable conductive hydrogel ink

To prepare the conductive hydrogel ink, 1.5 g of abovementioned filtered hydrogel matrix was added into a 12 mL Thinky container, followed by adding a certain amount of Ag flakes (1.487 g (7.5% volume ratio), 1.820 g (9% volume ratio), 2.275 g (11% volume ratio), 2.671 g (13% volume ratio), 3.238 g (15% volume

ratio), 3.3 g (17% volume ratio)). The ink was mixed using Thinky planetary mixer (2000 rpm, 1.5 min) for 3 times. The obtained ink was further mixed with 0.1% wt percentage of defoaming agent (XS-101) to form conductive hydrogel ink. The obtained printable conductive hydrogel ink was sealed and could be stored in either room temperature or 4 ºC. Before printing, the ink needs to be loaded into a 3 c.c. syringe and centrifuged at 3500 rpm for 15 min (Neofuge 1600, HealForce) two times to degas (Supplementary Fig. 22).

Preparation of printable conductive hydrogel ink with a random distribution of Ag flakes

0.05 g of PEO (1000 kDa) was dissolved in 1g of MEA/HEA monomer micelle solution (water-to-monomer ratio of 2.6). The mixture was then mixed with 2.2 g of Ag flakes using a planetary mixer at 2000 rpm for 1 min. 0.014 g of defoaming reagent XS-101 was then added and mixed with the ink, forming a printable conductive hydrogel ink with a random distribution of Ag flakes. The ink was further centrifuged at 2200 rpm for 5 min to degas before use.

Rheological measurement

All the rheological measurements were determined with a controlled stress rheometer (DHR-3, TA Instruments, New Castle, DE), using a 25-mm-diameter plane plate with a 300 μm gap between the parallel plates at 25 ºC. The viscosities of samples were measured using a steady shear rate increasing from 0.001 to 1,000 $s^{-1}$ at a frequency of 1 Hz. The storage and loss modulus measurements were performed in an oscillatory mode, in which the stress amplitude ranged from 0.1 to 3,000 Pa at a stress sweep with a frequency of 1Hz.

Conductivity measurement

For conductivity measurement, the conductive hydrogel ink with a varying of Ag flake volume ratio (7.5%, 9%, 11%, 13%, 15%, 17%) was embedded printed into a linear shape (length=18 mm, linewidth = 200 μm) with two pads exposed on top. The prints were settled for a certain amount of time, then cured by a UV irradiation for 20 min, followed thermal curing at 82 ºC for 1 hour. The resistance of the conductive hydrogel of both its original and swollen state was measured by a LCR meter (E4980AL, Keysight). The length and linewidth of swollen samples were determined by micrometer caliper and optical microscopy, respectively. Each sample was repeated at least 10 times. The conductivity ($\sigma$) was calculated as

$$\sigma = \frac{L}{R\pi\left(\frac{D}{2}\right)^2} \quad (2)$$

Where *L* was the length of printed conductive hydrogel, *R* was the measured resistance, *D* was the diameter of the printed conductive hydrogel.

Fabrication and characterization of wireless hydrogel electronics

The custom-designed acrylic mold (Supplementary Fig. 24a) for wireless hydrogel inductor was printed using a micro 3D printing system (BMF Precision Technology Co, Ltd., nanoArch S140). After washing and drying the printed acrylic molds, the demolding reagent was sprayed onto them before EM3DP. To fabricate wireless hydrogel inductors, the supporting matrix was degassed and loaded into a printed acrylic mold. EM3DP of conductive hydrogel ink with a Ag flake volume ratio of 17% was proceeded using our custom-built direct ink writing platform with the print path generated by G-code. After printing, the acrylic mold was covered by a glass coverslip and allowed to settle for 12 min. Thereafter, the prints were UV cured (~2.5 mW/cm$^2$) for 20 min, and then transferred to a heating plate curing at 82 ºC for 1 hour. The inductance of the wireless hydrogel inductors in both their original and swollen state were measured by a LCR meter (E4980AL, Keysight) at a frequency of 100 kHz. The output voltage ($V_{pp}$) and biphasic output waveforms of hydrogel inductor was measured by an ENA Vector Network Analyzer (N5071C, Keysight).

To fabricate AS-hydrogel based optoelectronic devices, a μLED was first modified using our previously reported approaches[1]. The optoelectronic device was then printed inside a custom-design acrylic mold (Supplementary Fig.24b) using our custom-built 3D printer. The printed optoelectronic device was allowed to settle for 14 min and then cured sequentially by a 365 UV light for 20 min and a thermal curing process at 82 for 1 hour. The optoelectronic device was dialyzed in deionized water for 3 days and swollen to equilibrium before use.

To implant the AS-hydrogel based wireless optoelectronic device, the device was sterilized using 75% ethanol washing twice, followed by UV irradiation for 30 min. A 1cm incision was made on the rat's chest, and the skin was bluntly separated. Then, an AS-hydrogel based wireless optoelectronic device was implanted under the skin of the rat.

Wireless power transfer system

The transmitter of the wireless power transfer (WPT) system consists of a DC voltage source $U_{dc}$, a half-bridge inverter $S_1$, $S_2$, (Wolfspeed C3M0040120K), a resonant capacitor $C_t$, and a transmission coil $L_t$. The system

works at 100 kHz which is modulated by the half-bridge inverter, $L_t$ and $C_t$ are resonant at the working frequency f according to eq. (3).

$$2\pi f L_t = \frac{1}{2\pi f C_t} \tag{3}$$

Then, the hydrogel receiving coil Lr can generate the induced voltage by magnetic coupling, which the mutual inductance M represents in the figure. The resistance of the receiving coil is represented by Rr. The diode D, wrapped by the hydrogel on the receiving side, is used for half-bridge rectification to convert the AC induction power to DC to the electrode (Supplementary Fig. 25).

Fabrication of all-hydrogel brain computer interface (BCI)

To fabricate all-hydrogel brain computer interface, certain amounts of supporting matrix was degassed and loaded into a printed mold (Supplementary Fig. 26a). The all-hydrogel BCIs were printed using a conductive hydrogel ink with a Ag flake volume ratio of 17%. The prints were covered by glass coverslips and allowed to settle for 12 min. Then the prints were UV cured for 20 mins and thermal cured for another 1 hour. The printed all-hydrogel BCIs were then assembled with a 12 pin connector via a AgTPU conductive ink. After drying the AgTPU ink at 80 ºC. The all-hydrogel BCIs were dialyzed in deionized water for 2 days and sterilized using 75% ethanol washing twice, followed by a UV irradiation for 30 min.

*In vivo* brain surgeries

After scalp incision and tissue cleaning, the skull was exposed, and the sensorimotor cortex (2.95 mm anteroposterior, 1.65 mm mediolateral relative to Bregma) was identified as the center of a skull window near the hindlimb representation area. (5 mm × 5mm)

To access the cortex, the skull and dura mater were carefully removed. The hydrogel electrode was placed directly onto the exposed cortex, covered with a glass coverslip, and secured to the skull with medical glue. A 0.8 mm hole was drilled near the Lambda for a ground screw. The hydrogel electrode and ground screw were connected to a pin connector and fixed with dental cement for stability during signal recording. After wound suturing, the rat was kept in a warm box until it recovered and was allowed to rest for six days before further procedures.

*In vivo* recording of the somatosensory evoked potentials with muscle stimulation

The ECoG data were recorded from anaesthetized rat models using a neural recording data acquisition system (Plexon, OmniPlex). A monophasic electrical stimulation (0.25 Hz, 1V) was delivered to the medial gastrocnemius muscle of the contralateral hindlimb using stainless steel wires (AS632, Cooner Wire, USA). On 1 week and 1-month post-implantation, the ECoG signals were recorded and amplified with a gain of 1,750 using the neural signal acquisition system, sampled at 40 kHz, and processed with a 2-500 Hz band-pass filter (fourth-order Butterworth) and a 50 Hz notch filter. Data were segmented based on the stimulation onset time (1200 ms). Sixty-sweep averages were mean-corrected for further analysis using MATLAB (2020b).

Fabrication and characterization of AS-hydrogel based wireless sciatic nerve stimulator

The custom-designed acrylic molds (Supplementary Fig. 26b) were printed using a micro 3D printing system (BMF Precision Technology Co, Ltd., nanoArch S140). After washing and drying the printed acrylic molds, the demolding reagent was sprayed onto them before EM3DP. The surface mount Schottky barrier rectifiers (marketing code: S14) were modified according to our previously reported methods. To fabricate AS-hydrogel based wireless sciatic nerve stimulator, the supporting matrix was degassed and loaded into the acrylic mold, the modified rectifier was placed at targeted position using our custom-made 3D printer. The 3D printing path of sciatic nerve stimulator was generated by G-code and was printed using a conductive hydrogel ink with a Ag flake volume ratio of 17%. The prints were covered by glass coverslips and allowed to settle for 12 min. The prints were further UV and thermal cured, followed by dialyzing in deionized water for 3 days. The output voltages ($V_{pp}$) of the AS-hydrogel based wireless sciatic nerve stimulators were measured by an ENA Vector Network Analyzer (N5071C, Keysight) at 2 cm. The devices were further sterilized using 75% ethanol washing, followed by a UV irradiation for 30 min.

*In vivo* sciatic nerve surgeries

A 2 cm incision was made on the skin of the rat's hindlimb, exposing the subcutaneous tissue. The sciatic nerve was exposed by separating the muscles close to the femur. The electrodes was wrapped around the surface of the exposed sciatic nerve, while the receiving coil was inserted through the incision and implanted under the skin. For the sham group, Ecoflex-30 mock device was implanted. One sample was implanted per animal for right hindlimb.

Long-term *in vivo* rat sciatic nerve stimulation

On day 1 and week 1 post-implantation, the implanted rats were anaesthetized by using inhaled isoflurane. The transmitting coil was connected to our custom-built near field wireless powering system and was placed right above the implanted hydrogel receiving coils. The input voltage was set at 30, 36, 40, 43 V (1Hz) to generate 400, 500, 550, 600 mV output voltages on rat sciatic nerve, triggering the leg motion. A protractor marker was placed under rat's hindlimb to measure the leg motion.

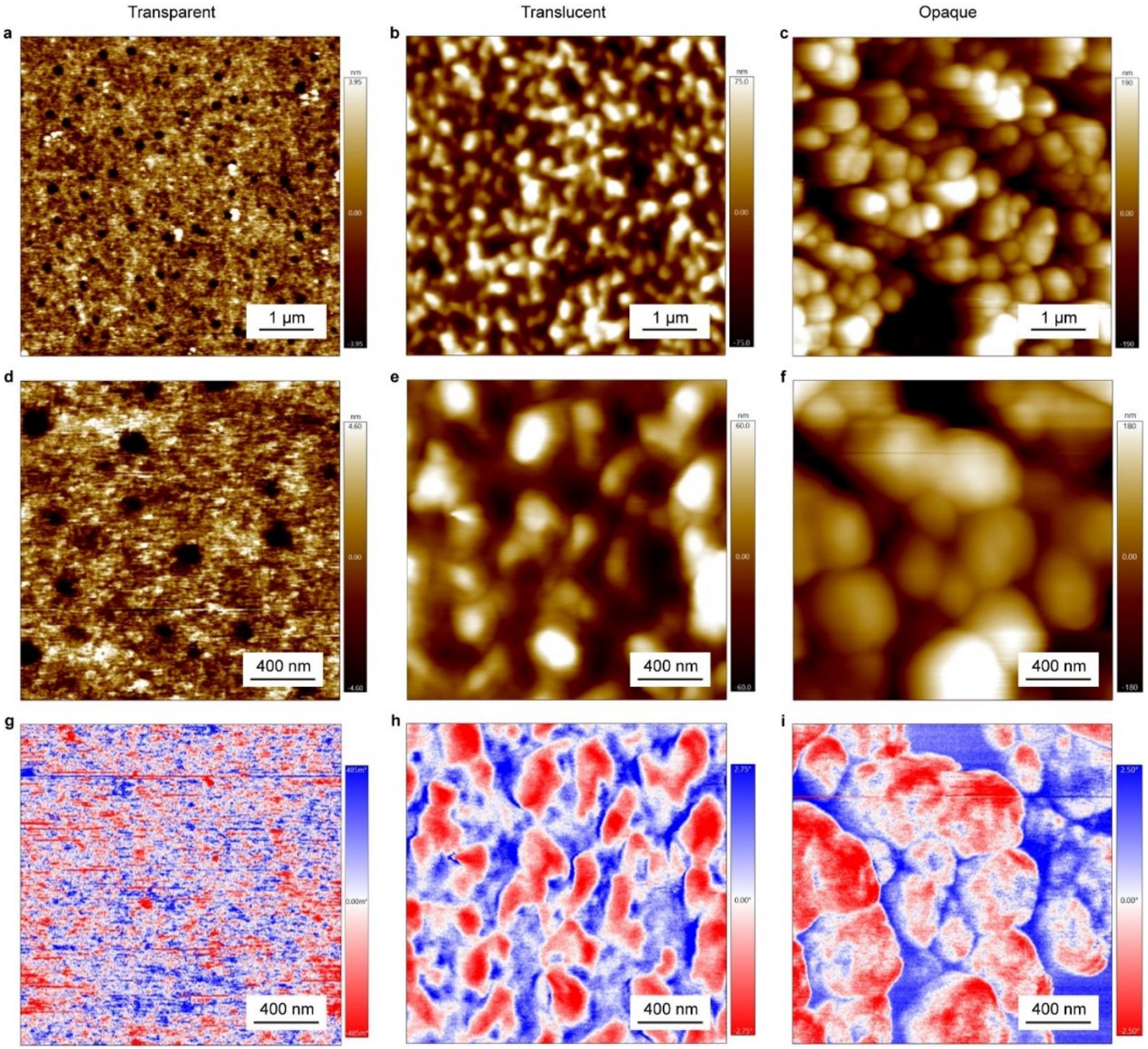


**Supplementary Fig. 1 | The AFM images of PHEA-PEA AS-hydrogels. a, d, g,** The AFM image, zoomed-in the AFM image and the phase image of swollen transparent PHEA-PEA AS-hydrogel. **b, e, h,** The AFM image, zoomed-in the AFM image and the phase image of swollen translucent PHEA-PEA AS-hydrogel. **c, f, i,** The AFM image, zoomed-in the AFM image and the phase image of swollen opaque PHEA-PEA AS-hydrogel.

**Supplementary Discussion 1. The formation mechanism of micelle-assembly anti-swelling hydrogels**

We hypothesized that the HEA/EA combination (with a fixed molar ratio of 2:1) was functioned like a monolithic surfactant, where the relatively long-chain HEA molecules acted as hydrophilic tails, and the comparably short-chain EA molecules acted as hydrophobic heads (Fig. 1b). Upon mixing with water, the hydrophilic tails, aka the HEA molecules, formed hydrophilic coronas, while the hydrophobic heads, aka the EA molecules, were associated to form hydrophobic cores, therefore producing homogenous monomer micelle solutions. The SANS was adopted to investigate the monomer micelle solutions. Supplementary Fig. 2 showed the SANS profiles and 2D scattering patterns of the monomer micelle solutions with varying water-to-monomer molar ratios. The morphology of micelle was perfectly fitted by using a cylinder-shaped model and the detailed morphological information was listed in Supplementary Table 1. We noticed that the monomer micelle solutions with different water-to-monomer molar ratios exhibited nearly identical diameters ranging from 1.05 to 1.36 nm. However, the length of cylinder-shaped micelles was sharply decreased from ~10 to 2.7 nm, along with the lowering of water-to-monomer molar ratios (increasing of micelle concentrations). We found this morphological evolution was identical to highly concentrated micelle solutions (above its critical micelle concentration). Where the increasing of surfactant concentration resulted in a subsequential micellar morphological transition from cylinder-shape to disk-shape, accompanied by a gradual decrease of micellar length. In addition, the Guinier regions (low q region) of micelle solutions were all flatten, indicating the micelles were stably dispersed without forming larger aggregates before curing.

Supplementary Fig. 3 compared the SANS profiles and 2D patterns of the swollen AS-hydrogels prepared by direct UV curing of monomer micelle solutions. The minimum feature size of AS-hydrogel with a water-to-monomer molar ratio of 4 was calculated as 1.25 nm radially and 4.65 nm longitudinally. The decrease in feature size longitudinally might resulted from the self-assembly process of the cylinder-shaped micelles during polymerization. Where the cylindrical micelles were tended to partially merge and aggregate to minimize their surface energy, forming hydrogel with hierarchical structures. The slope factor in its Guinier region was calculated as ~ -4, further proved this hypothesis (Supplementary Fig.3a). Whereas the minimum feature size of AS-hydrogel with a water-to-monomer molar ratio of 2 was calculated as 1.17 nm radially and 3.54 nm longitudinally, only showing a slightly increase in both dimensions, suggesting that the monomer micelles with a morphology intermediate between a cylinder and a disk were favorable for *in-situ* gelation.

We further monitored the hydrogel formation process of an opaque AS-hydrogel using both photography and microscopic imaging (Supplementary Fig. 4). Throughout the UV curing process, the precursor transitioned from a transparent state to an opaque hydrogel, accompanied by the formation of particular-shaped aggregates (Supplementary Fig. 4e). These aggregates exhibited a particle size in the several micrometer range, consistent with the AFM image presented in Supplementary Fig. 1c (the insert in Supplementary Fig. 4f). We assigned these particular-shaped aggregates to the clusters of assembled micelles. The aggregates were subsequently adhered to each other to create gelled precursors (Supplementary Fig. 4f). The curing process of the transparent AS-hydrogel was also observed. No macroscopic changes were observed

throughout the entire curing process. The observations once more validated our hypothesis.

**Supplementary Table 1 | Theoretical calculated the morphological information of monomer precursor and AS-hydrogels**

| Sample | | Morphological parameters | | |
|---|---|---|---|---|
| | Water-to-monomer molar ratio (*W*) | Diameter (nm) | Length (nm) | Polydispersity |
| Monomer micelle solution | 4.0 | 1.36 | 10.03 | 0.065 |
| | 3.0 | 1.23 | 8.52 | 0.065 |
| | 2.1 | 1.05 | 2.70 | 0.013 |
| AS-hydrogel | 4.0 | 1.25 | 4.65 | N/A |
| | 3.0 | 1.18 | 3.90 | N/A |
| | 2.1 | 1.17 | 3.54 | N/A |

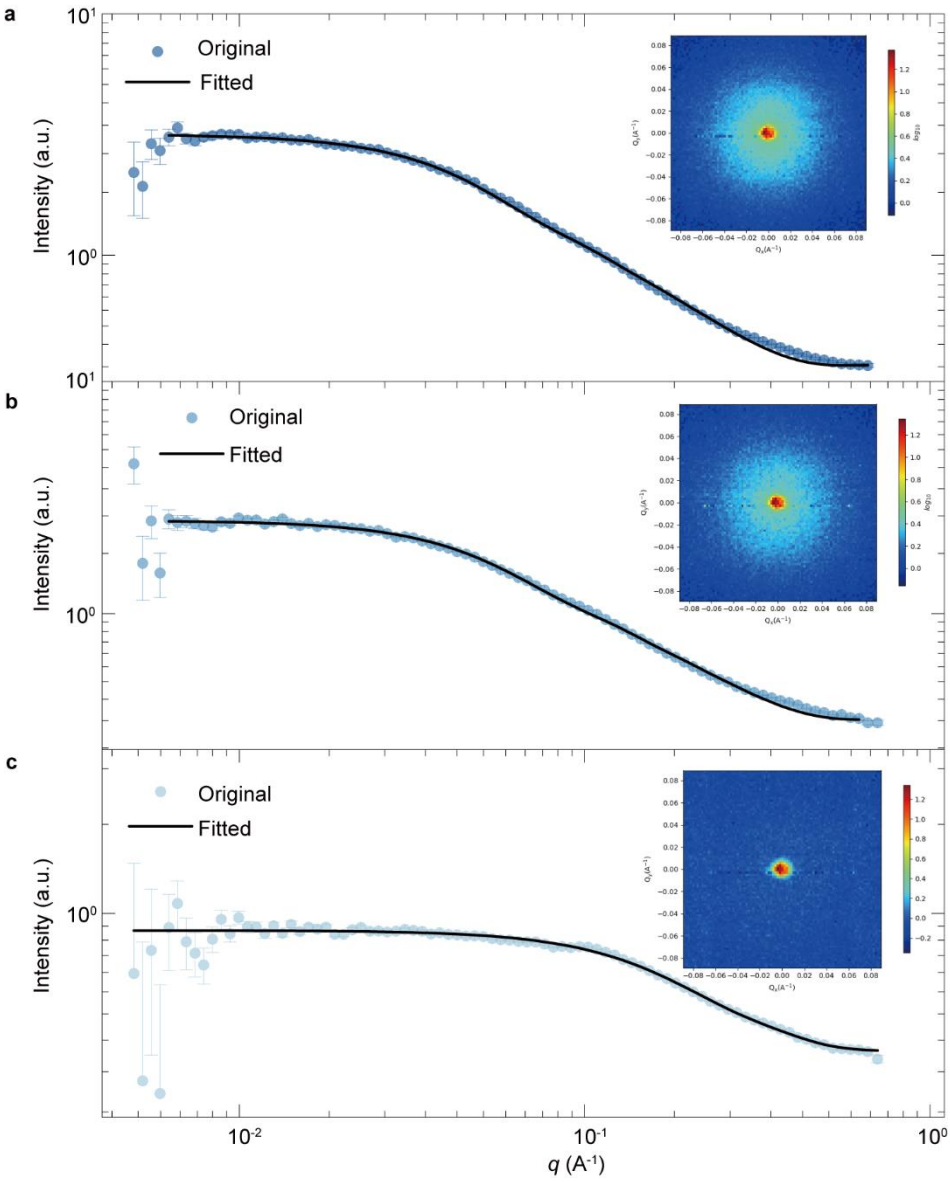


**Supplementary Fig. 2 | The original and fitted SANS profiles of monomer precursors. a,** The original and fitted SANS profile of monomer precursor with a water-to-monomer molar ratio of 4, insert is the 2D SANS pattern. **b,** The original and fitted SANS profile of monomer precursor with a water-to-monomer molar ratio of 3, insert is the 2D SANS pattern. **c,** The original and fitted SANS profile of monomer precursor with a water-to-monomer molar ratio of 2.1, insert is the 2D SANS pattern.

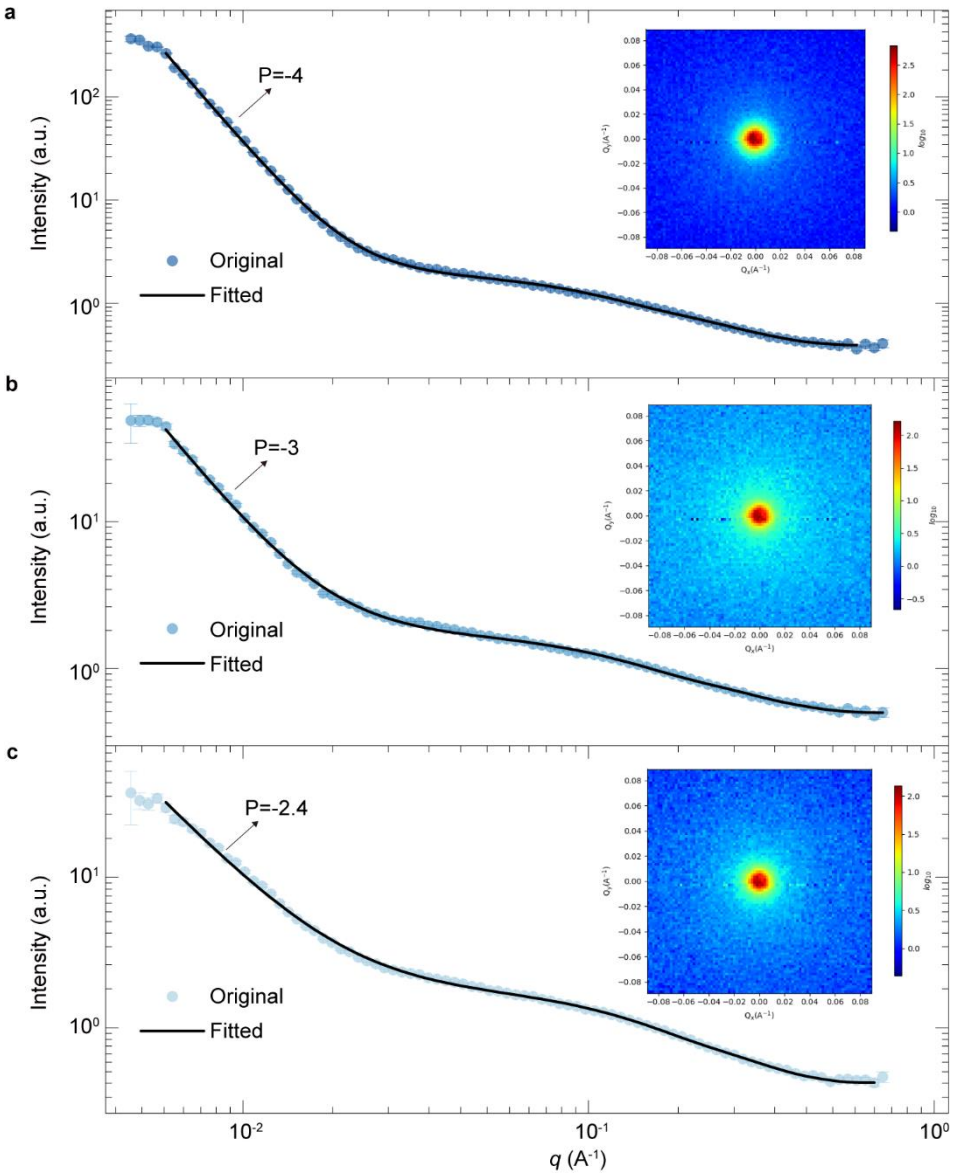


**Supplementary Fig. 3 | The original and fitted SANS profiles of AS-hydrogels. a,** The original and fitted SANS profile of AS-hydrogel with a water-to-monomer molar ratio of 4, insert is the 2D SANS pattern. **b,** The original and fitted SANS profile of AS-hydrogel with a water-to-monomer molar ratio of 3, insert is the 2D SANS pattern. **c,** The original and fitted SANS profile of AS-hydrogel with a water-to-monomer molar ratio of 2.1, insert is the 2D SANS pattern.

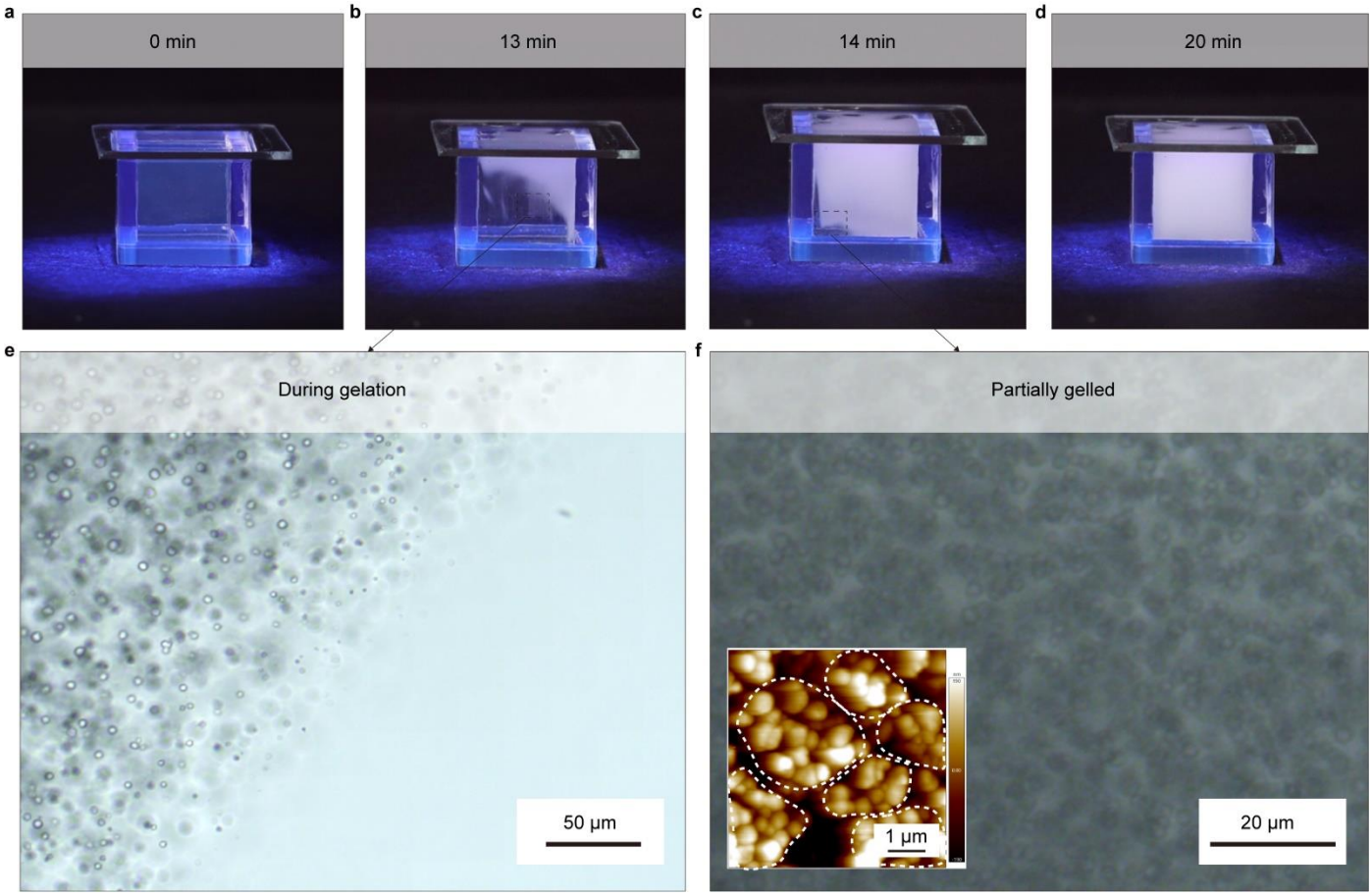


**Supplementary Fig. 4 | The *in-situ* monitoring of hydrogel formation process of an opaque AS-hydrogel.** **a**, **b**, **c**, **d**, The photographic recording of hydrogel formation process at different time interval (0, 13, 14, 20 min). **e**, The optical microscopic image of hydrogel formation process at a time interval of 13 min. **f**, The optical microscopic image of hydrogel formation process at a time interval of 14 min, insert shows the AFM images of cured AS-hydrogels.

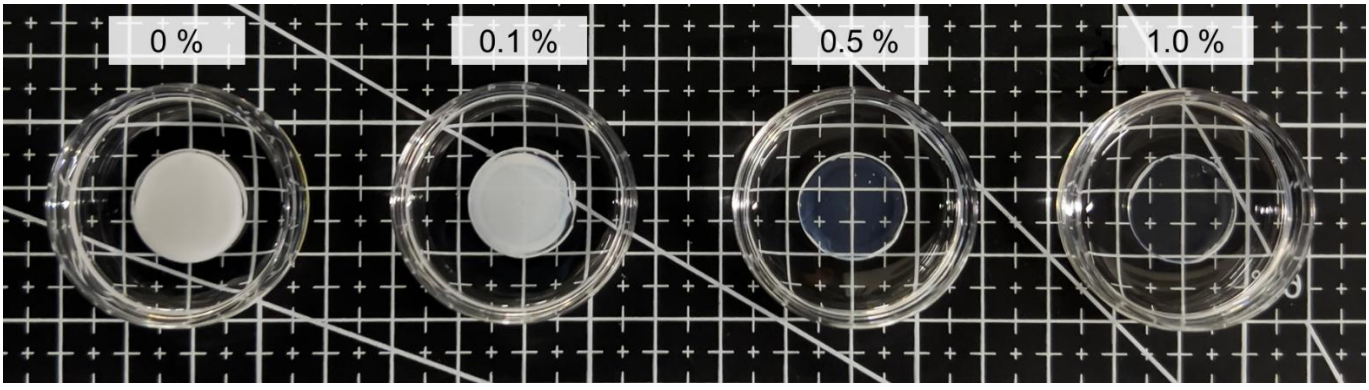


**Supplementary Fig. 5 | Increasing of crosslinking prevent the self-assembly process during UV curing.** The digital photo of PHEA-PEA AS-hydrogel ($W$=4) with varying EGDMA crosslinking density (left to right: without, 0.1%, 0.5% and 1%).

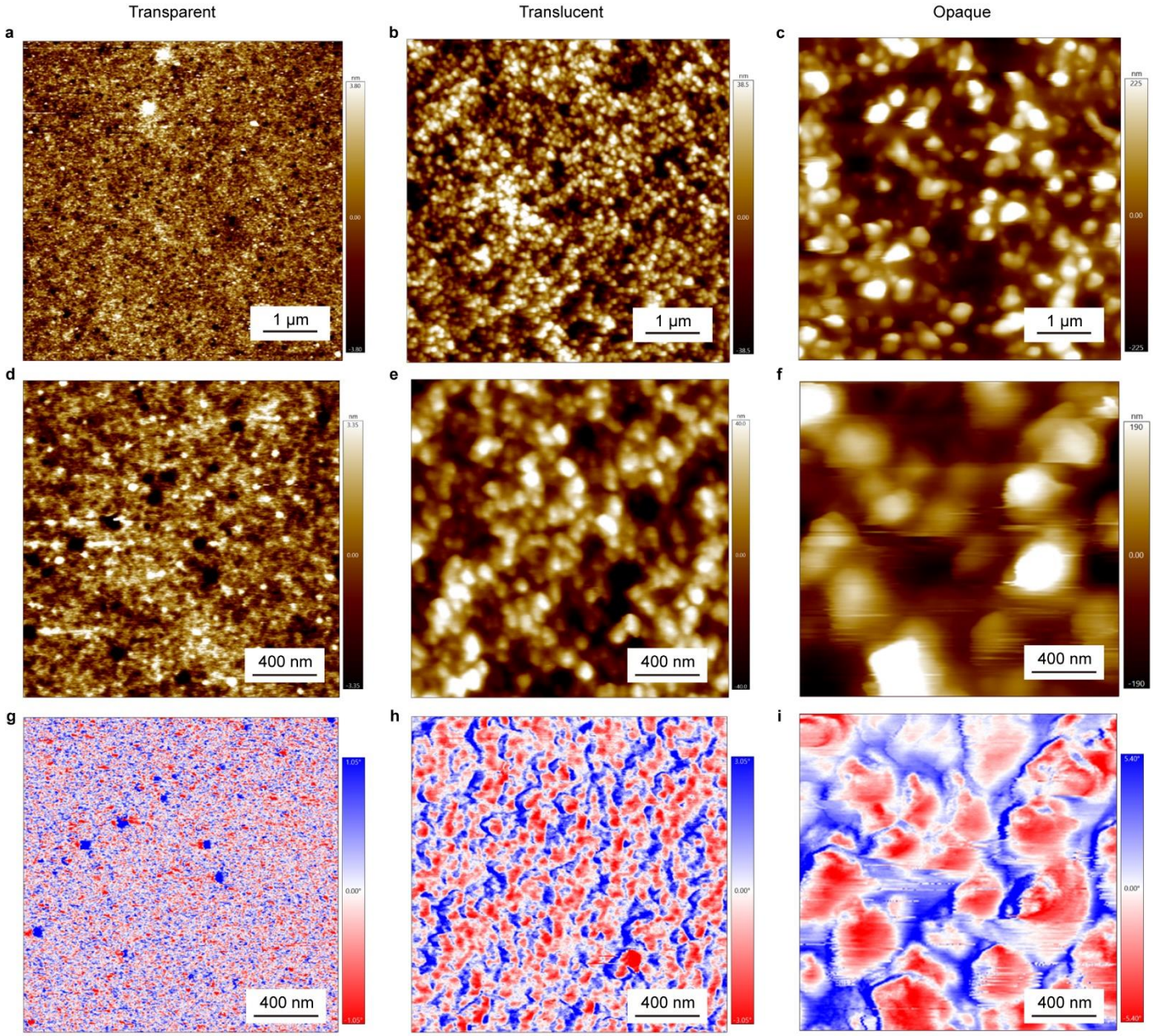


**Supplementary Fig. 6 | The AFM images of PHEMA AS-hydrogels. a, d, g,** The AFM image, zoomed-in the AFM image and the phase image of swollen transparent PHEMA AS-hydrogel. **b, e, h,** The AFM image, zoomed-in the AFM image and the phase image of swollen translucent PHEMA AS-hydrogel. **c, f, i,** The AFM image, zoomed-in the AFM image and the phase image of swollen opaque PHEMA AS-hydrogel.

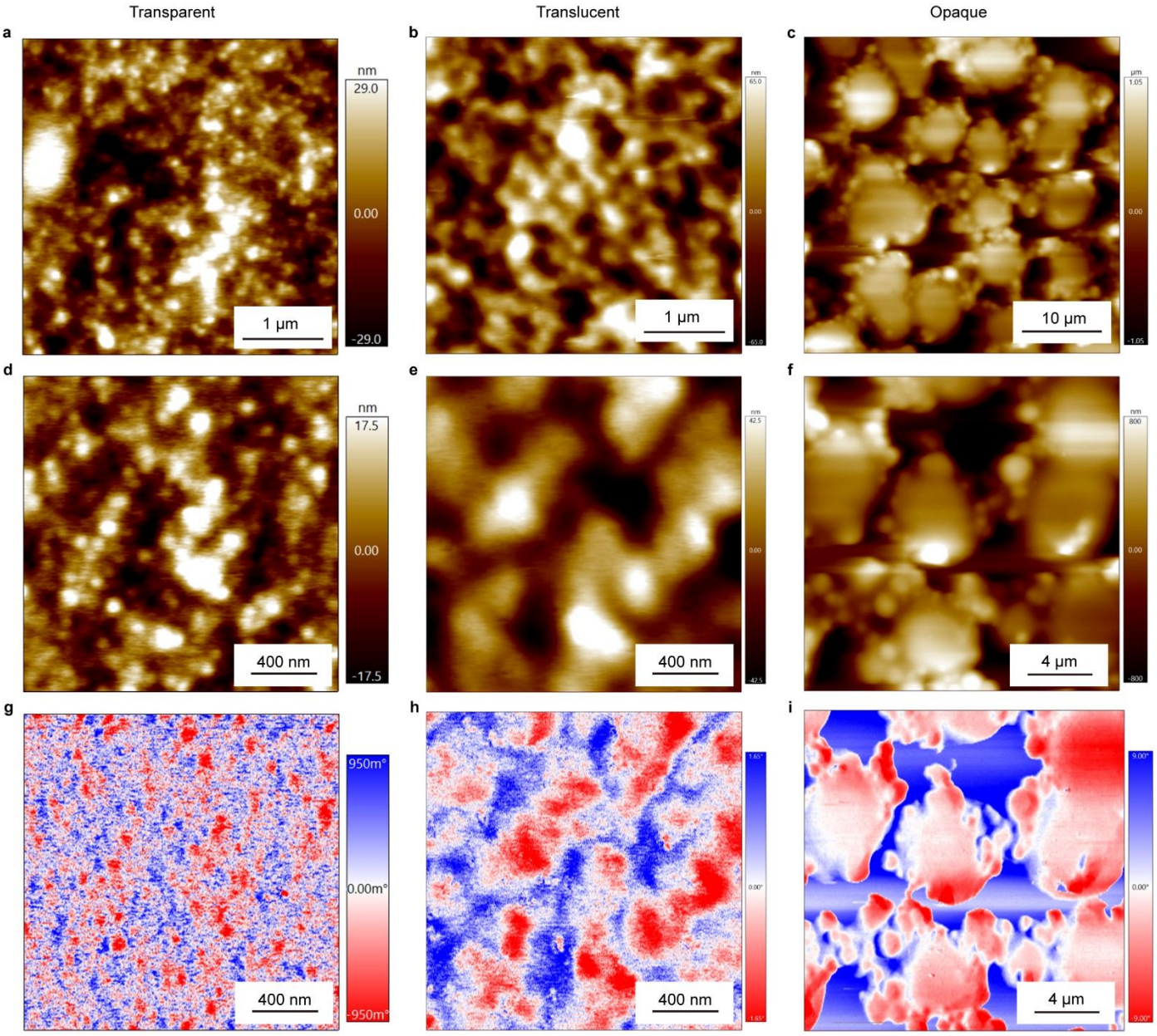


**Supplementary Fig. 7 | The AFM images of PMEA-PHEA AS-hydrogels. a, d, g,** The AFM image, zoomed-in the AFM image and the phase image of swollen transparent PMEA-PHEA aS-hydrogel. **b, e, h,** The AFM image, zoomed-in the AFM image and the phase image of swollen translucent PMEA-PHEA AS-hydrogel. **c, f, i,** The AFM image, zoomed-in the AFM image and the phase image of swollen opaque PMEA-PHEA AS-hydrogel.

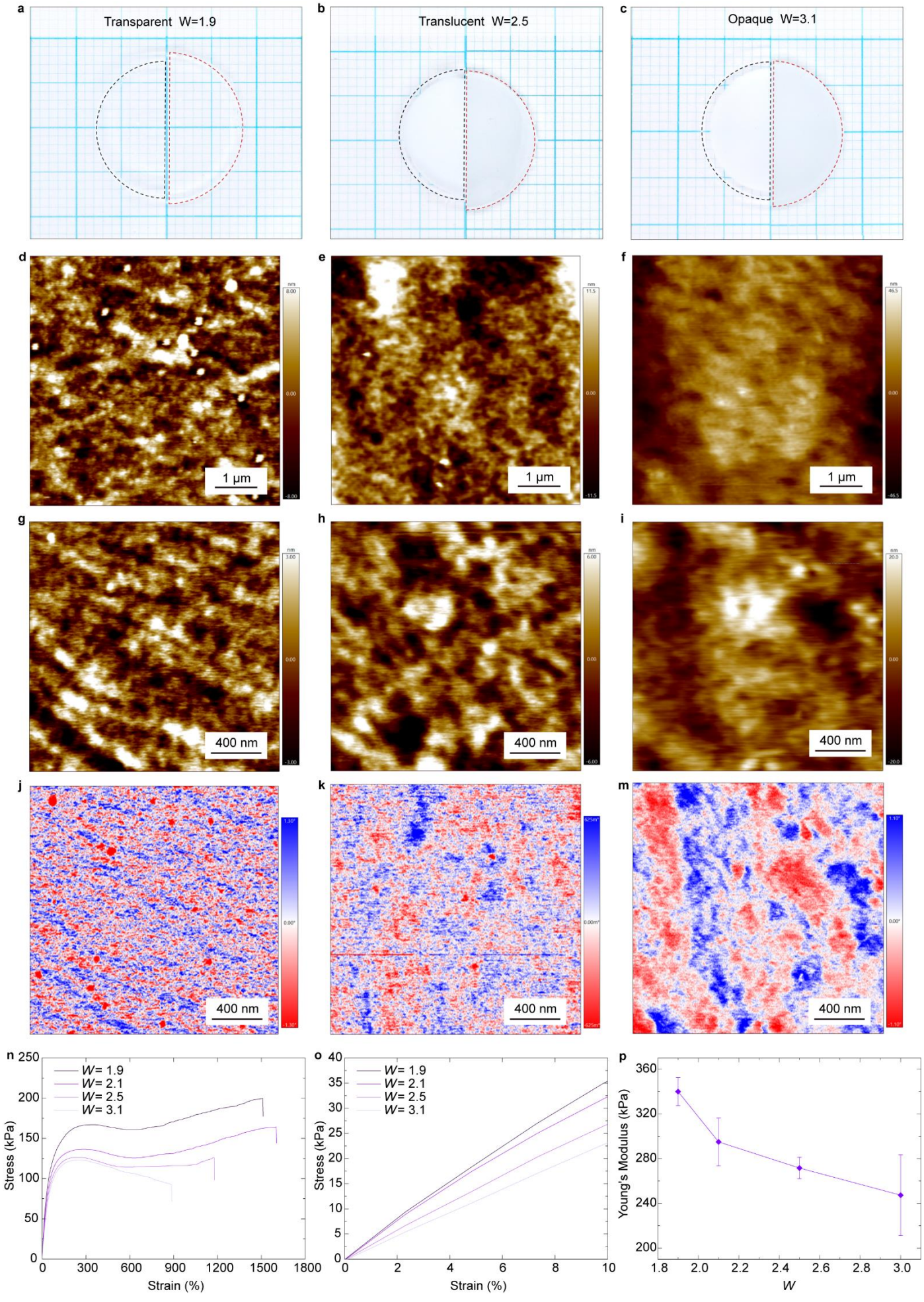


**Supplementary Fig. 8 | The Macroscopic morphologies, AFM images and mechanical performances of**

**PAA-PAM-PEA AS-hydrogels. a,** The digital image of as-prepared (left) and swollen (right) transparent PAA-PAM-PEA AS-hydrogel. **b,** The digital image of as-prepared (left) and swollen (right) translucent PAA-PAM-PEA AS-hydrogel. **c,** The digital image of as-prepared (left) and swollen (right) opaque PAA-PAM-PEA AS-hydrogel. **d, g, j,** The AFM image, zoomed-in the AFM image and the phase image of swollen transparent PAA-PAM-PEA AS-hydrogel. **e, h, k,** The AFM image, zoomed-in the AFM image and the phase image of swollen translucent PAA-PAM-PEA AS-hydrogel. **f, i, m,** The AFM image, zoomed-in the AFM image and the phase image of swollen opaque PAA-PAM-PEA AS-hydrogel.

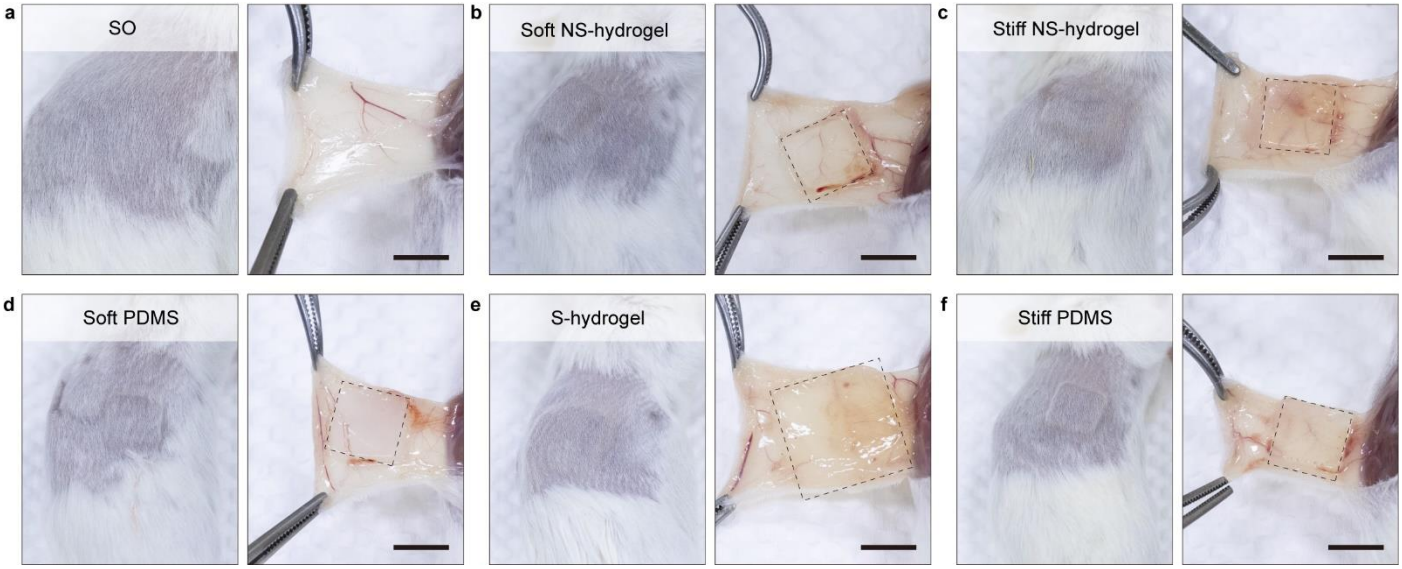


**Supplementary Fig. 9 | Representative images of implanted mice after 2 week implantation. a**, The sham operation group. **b**, The implanted soft NS-hydrogel group. **c**, The implanted stiff NS-hydrogel group. **d**, The implanted soft PDMS group. **e**, The implanted S-hydrogel group. f, The implanted stiff PDMS group.

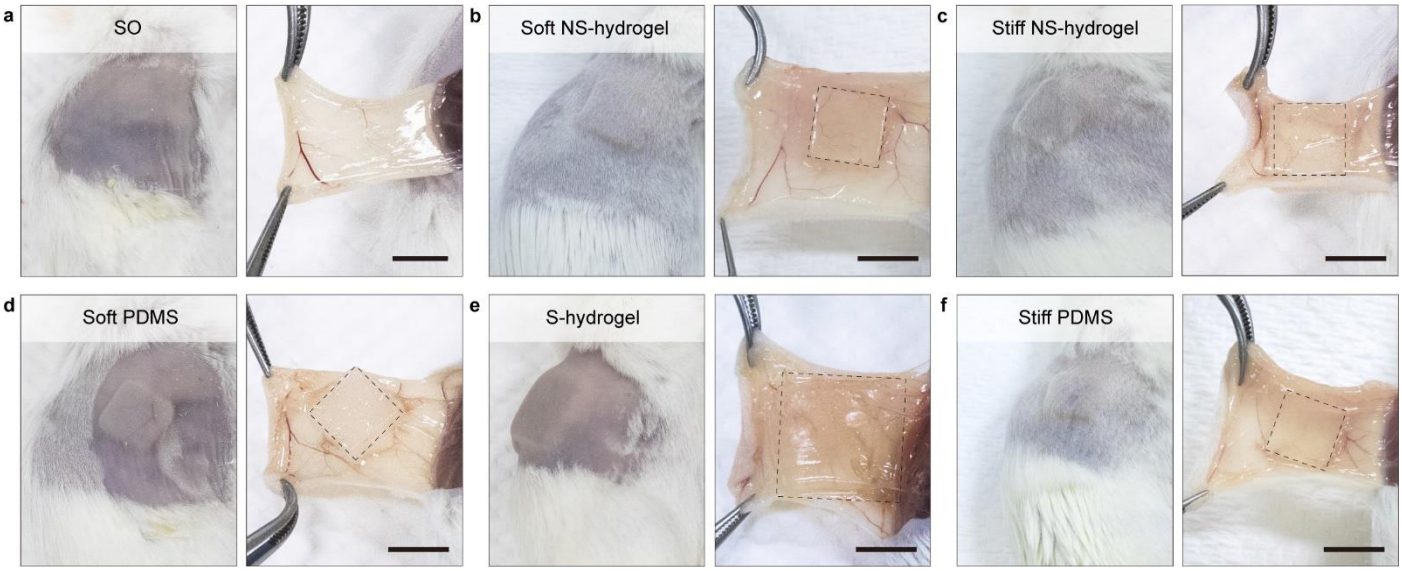


**Supplementary Fig. 10 | Representative images of implanted mice after 8 week implantation. a**, The sham operation group. **b**, The implanted soft NS-hydrogel group. **c**, The implanted stiff NS-hydrogel group. **d**, The implanted soft PDMS group. **e**, The implanted S-hydrogel group. f, The implanted stiff PDMS group.

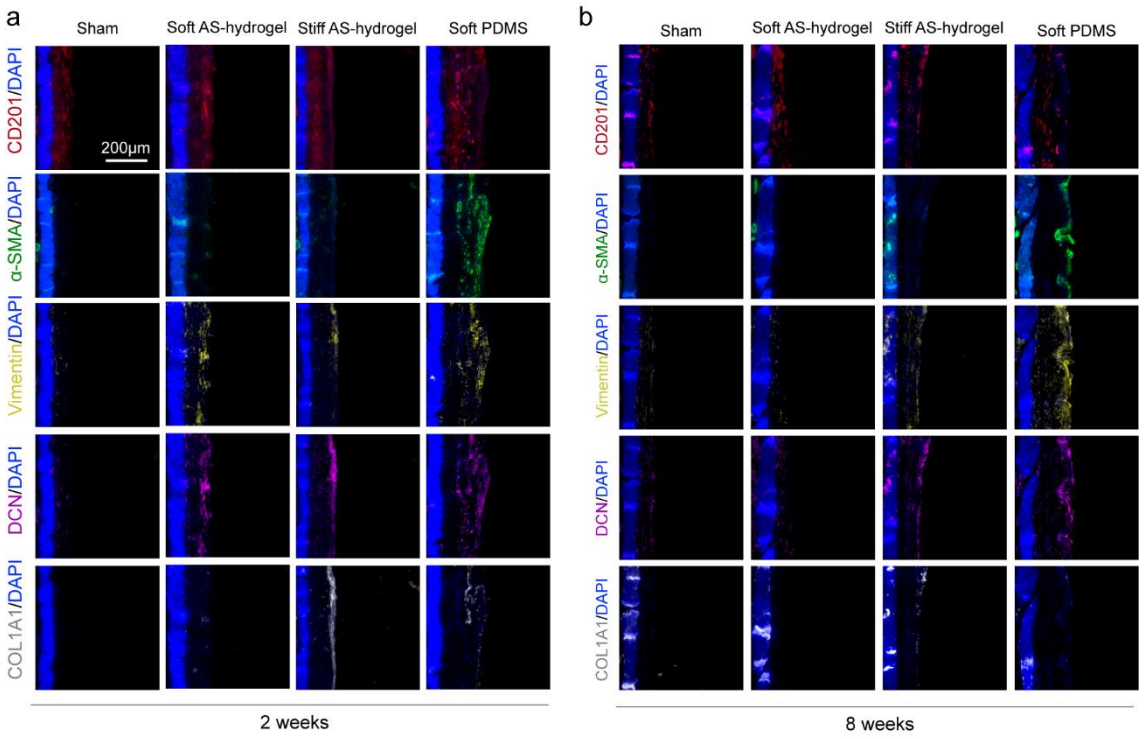


**Supplementary Fig. 11 | Multiple immunohistological imaging of the skin tissues adjacent to implanted mock devices. a**, Mouse skin tissues harvested after implantation 2 weeks were assessed for the multiplexed immunohistochemistry analysis (mIHC). Fibroblast is labeled with CD201/TSA650, α-SMA/TSA520, vimentin/TSA570, DCN/TSA660s, COL1A1/TSA 700 antibody. Scale bar=200 μm. **b**, Mouse skin tissues harvested after implantation 8 weeks were assessed for the mIHC. Fibroblast is labeled with CD201/TSA 650, α-SMA/TSA 520, vimentin/TSA 570, DCN/TSA 660s, COL1A1/TSA 700 antibody. Scale bar=200 μm.

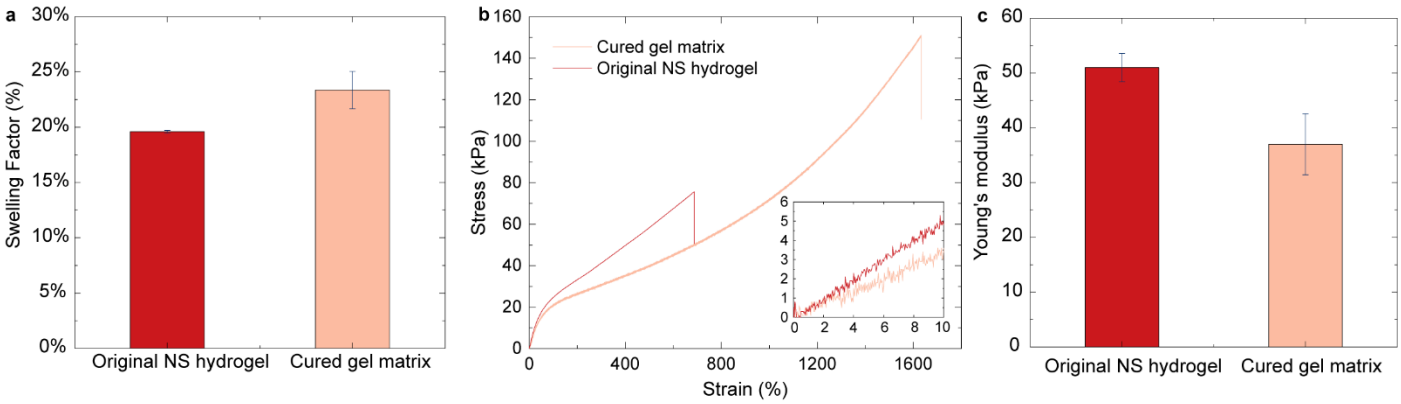


**Supplementary Fig. 12 | The comparison of swelling and mechanical properties of original AS-hydrogel and cured gel matrix.**

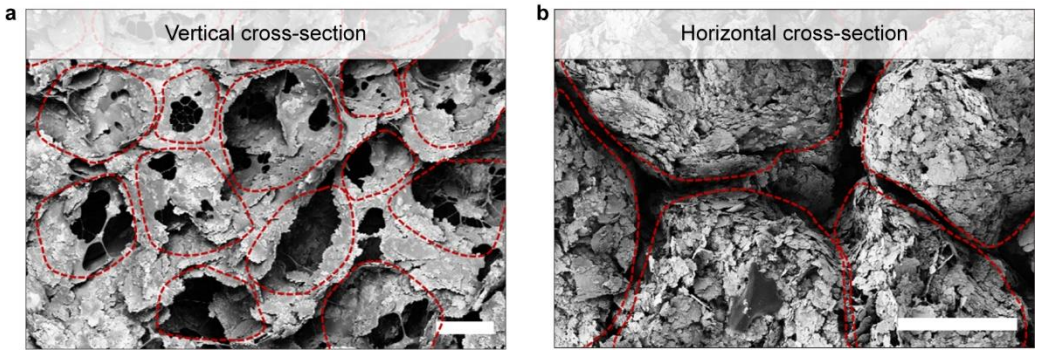


**Supplementary Fig. 13 | The SEM images of conductive hydrogel. a**, The vertical cross-section of conductive hydrogel. **b**, The horizontal cross-section of conductive hydrogel.

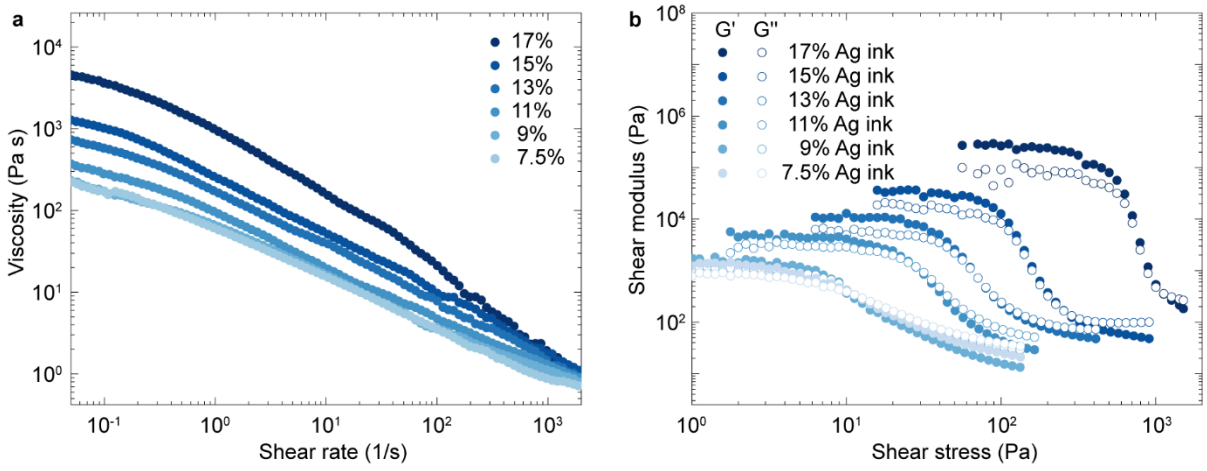


**Supplementary Fig. 14 | The rheological measurement of conductive hydrogel inks. a**, The viscosity as a function of shear rate of the conductive hydrogel ink with varying Ag flake volume ratios (7.5%, 9%, 11%, 13%, 15% and 17%) . **b**, The storage and loss moduli as a function of shear stress of the conductive hydrogel ink with varying Ag flake volume ratios (7.5%, 9%, 11%, 13%, 15% and 17%).

**Supplementary Fig. 15 | The digital image of conductive hydrogel ink with Ag flakes volume ratio above 17%.**

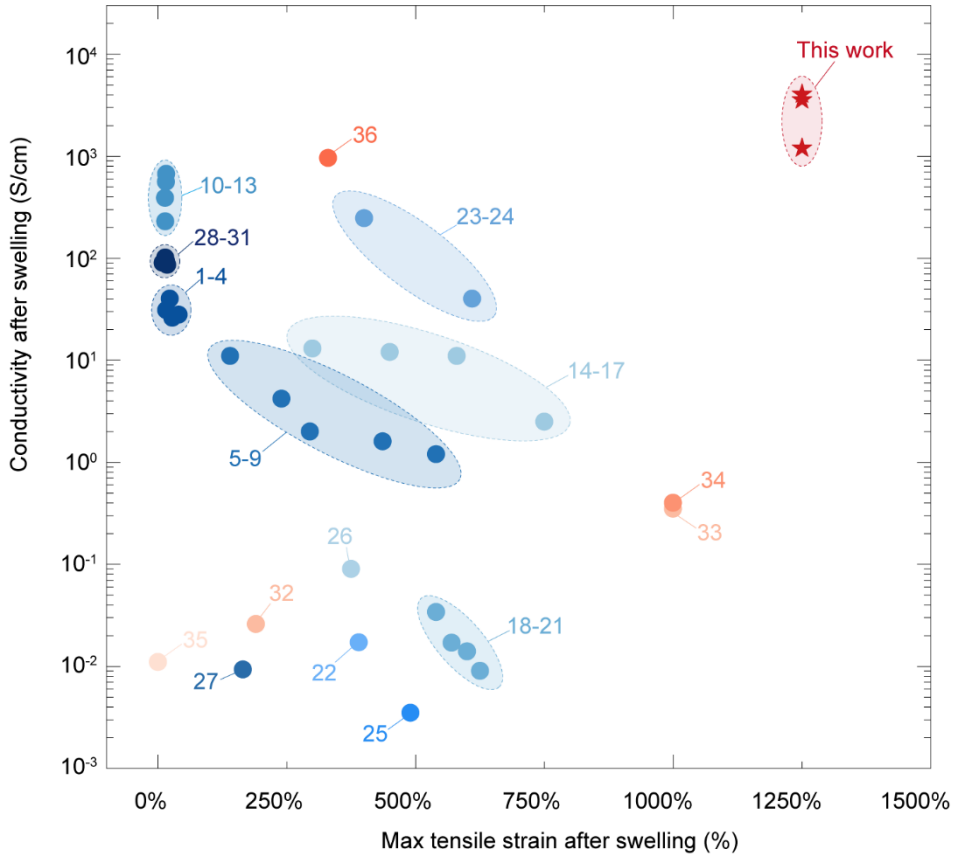


**Supplementary Fig. 16 | The Ashby plot of wet conductivity of conductive hydrogels.**

**Supplementary Table 2 | Ashby plot references**

| Data | Reference |
|---|---|
| **Conducting polymer-based conductive hydrogels** | |
| 1-4 | Lu, B., Yuk, H., Lin, S. et al. Pure PEDOT:PSS hydrogels. Nat Commun 10, 1043 (2019). [2] |
| 5-9 | G. Li, K. Huang, J. Deng, M. Guo, M. Cai, Y. Zhang, C. F. Guo, Highly Conducting and Stretchable Double-Network Hydrogel for Soft Bioelectronics. Adv. Mater. 2022, 34, 2200261.[3] |
| 10-13 | Daeyeon Won et al. Digital selective transformation and patterning of highly conductive hydrogel bioelectronics by laser-induced phase separation. Sci. Adv.8,eabo3209(2022).[4] |
| 14-17 | Zhou, T., Yuk, H., Hu, F. et al. 3D printable high-performance conducting polymer hydrogel for all-hydrogel bioelectronic interfaces. Nat. Mater. 22, 895-902 (2023).[5] |
| 18-21 | Z. Zhang, G. Chen, Y. Xue, Q. Duan, X. Liang, T. Lin, Z. Wu, Y. Tan, Q. Zhao, W. Zheng, L. Wang, F. Wang, X. Luo, J. Xu, J. Liu, B. Lu, Fatigue-Resistant Conducting Polymer Hydrogels as Strain Sensor for Underwater Robotics. Adv. Funct. Mater. 2023, 33, 2305705.[6] |
| 22 | Z. Sun, C. Dong, B. Chen, W. Li, H. Hu, J. Zhou, C. Li, Z. Huang, Strong, Tough, and Anti-Swelling Supramolecular Conductive Hydrogels for Amphibious Motion Sensors. Small 2023, 19, 2303612.[7] |
| 23-24 | Chong, J., Sung, C., Nam, K.S. et al. Highly conductive tissue-like hydrogel interface through template-directed assembly. Nat Commun 14, 2206 (2023).[8] |
| 25 | N. Li, Q. Yu, S. Duan, Y. Du, X. Shi, X. Li, T. Jiao, Z. Qin, X. He, Anti-Swelling, High-Strength, Anisotropic Conductive Hydrogel with Excellent Biocompatibility for Implantable Electronic Tendon. Adv. Funct. Mater. 2024, 34, 2309500.[9] |
| 26 | F. Wang, Y. Xue, X. Chen, P. Zhang, L. Shan, Q. Duan, J. Xing, Y. Lan, B. Lu, J. Liu, 3D Printed Implantable Hydrogel Bioelectronics for Electrophysiological Monitoring and Electrical Modulation. Adv. Funct. Mater. 2024, 34, 2314471.[10] |
| 27 | J. Dai, B. Wang, Z. Chang, X. Lu, J. Nie, Q. Ren, Y. Lv, M. Y. Rotenberg, Y. Fang, Injectable Mesh-Like Conductive Hydrogel Patch for Elimination of Atrial Fibrillation. Adv. Healthcare Mater. 2024, 13, 2303219.[11] |
| 28-31 | Won, D., Kim, H., Kim, J. et al. Laser-induced wet stability and adhesion of pure conducting polymer hydrogels. Nat Electron 7, 475-486 (2024).[12] |
| **Composite conductive hydrogels** | |
| 32 | Deng, J., Yuk, H., Wu, J. et al. Electrical bioadhesive interface for bioelectronics. Nat. Mater. 20, 229–236 (2021).[13] |
| 33 | Tringides, C.M., Vachicouras, N., de Lazaro, I. et al. Viscoelastic surface electrode arrays to interface with viscoelastic tissues. Nat. Nanotechnol. 16, 1019-1029 (2021).[14] |
| 34 | Y. Ohm, J. Liao, Y. Luo, M. J. Ford, C. Majidi, Reconfigurable Electrical Networks within a Conductive Hydrogel Composite. Adv. Mater. 2023, 35, 2209408.[15] |
| 35 | J. Park, J. Y. Kim, J. H. Heo, Y. Kim, S. A. Kim, K. Park, Y. Lee, Y. Jin, S. R. Shin, D. W. Kim, J. Seo, Intrinsically Nonswellable Multifunctional Hydrogel with Dynamic Nanoconfinement Networks for Robust Tissue-Adaptable Bioelectronics. Adv. Sci. 2023, 10, 2207237.[16] |
| 36 | Z. Wang, X. Xu, K. Zhang, R. Tan, S. Zhang, Y. Su, J. Hu, Continuous Phase Separation Induced Tough Hydrogel Fibers with Ultrahigh Conductivity for Multidimensional Soft Electronics. Adv. Funct. Mater. 2024, 2413478.[17] |

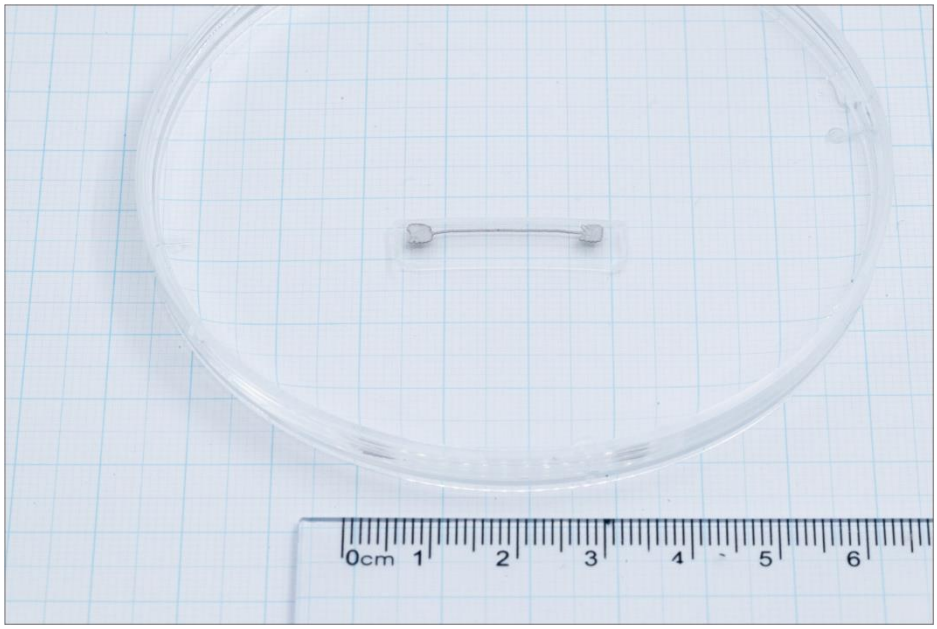


**Supplementary Fig. 17 | The printed linear resistor with a linewidth of 250 μm.**

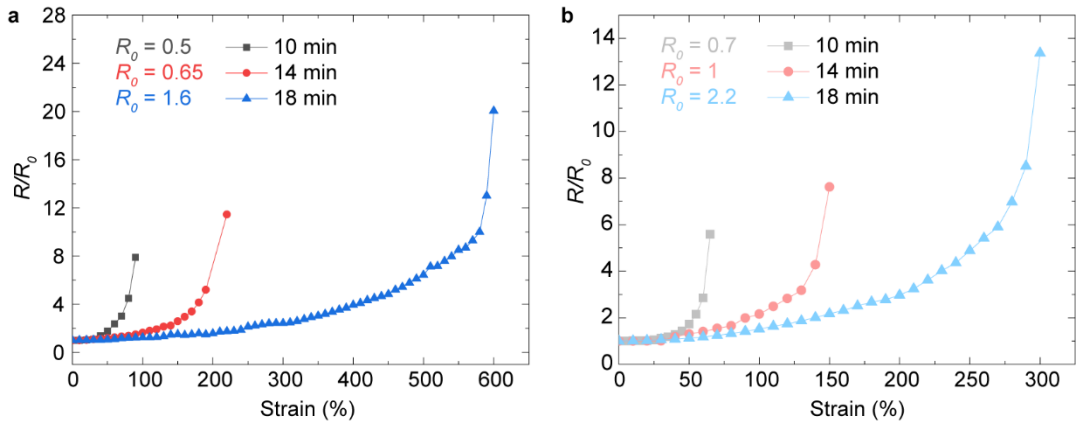


**Supplementary Fig. 18 | The electromechanical performance of printed linear resistor. a**, The normalized resistance ($R/R_0$) of printed linear hydrogel resistors in their original state. **b**, The normalized resistance ($R/R_0$) of printed linear hydrogel resistors in their swollen state.

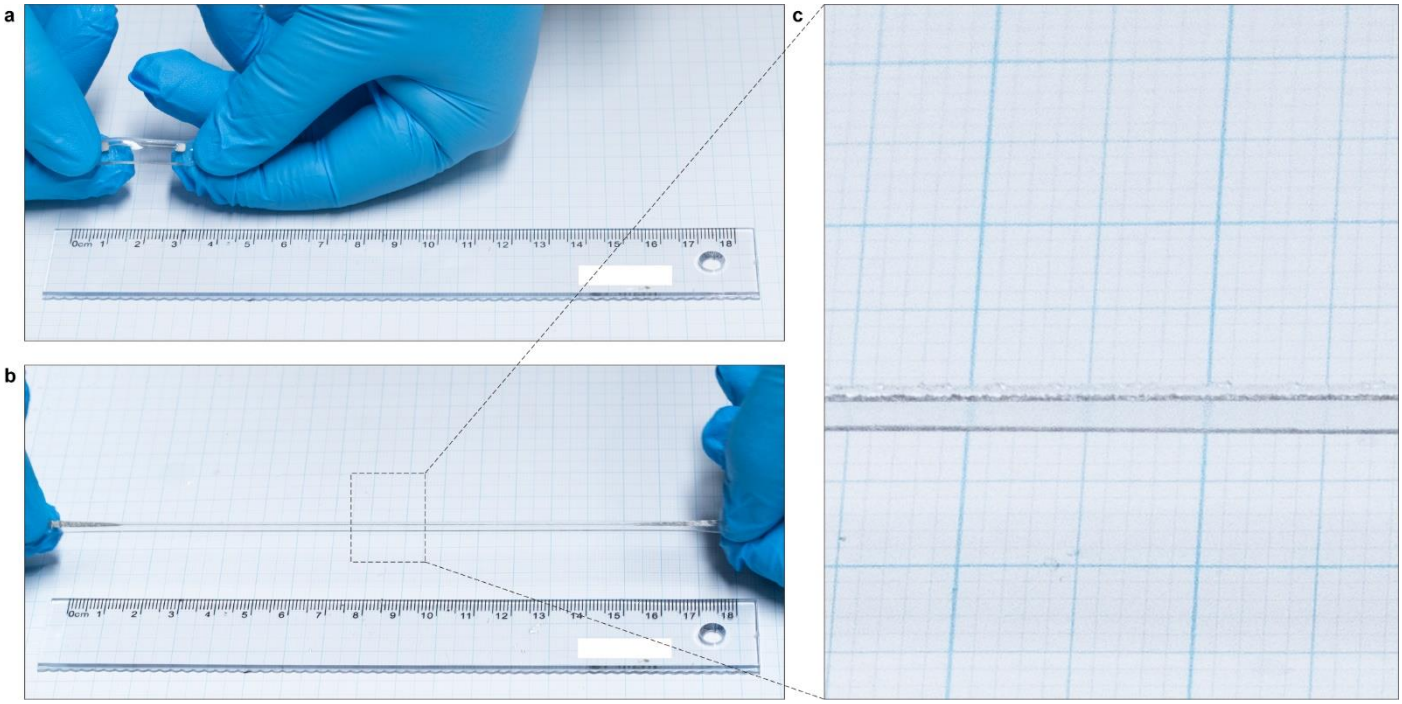


**Supplementary Fig. 19 | The high stretchability of swollen printed linear resistor. a**, The swollen printed linear hydrogel resistor. **b**, The swollen hydrogel resistor was stretched ~ 1,200% without breakage. **c**, The zoomed in photo showing that the printed conductive hydrogel filament was intact under a strain of ~ 1,200%.

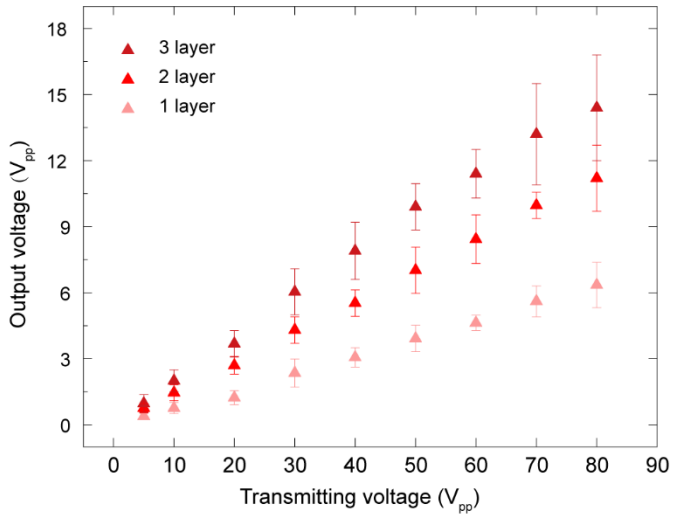


**Supplementary Fig. 20 | The comparison of output voltages generated by 2D and 3D inductors at varying transmitting voltages.**

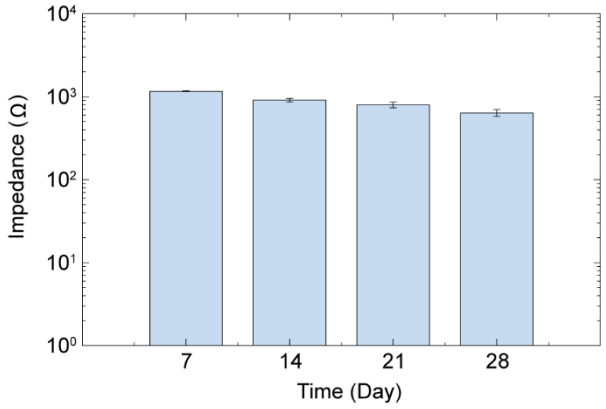


**Supplementary Fig. 21 | The *in-vivo in-situ* monitoring of impedance between electrodes and brain tissues over time.** The impedance was recorded at 1kHz between ground electrode and detection electrodes.

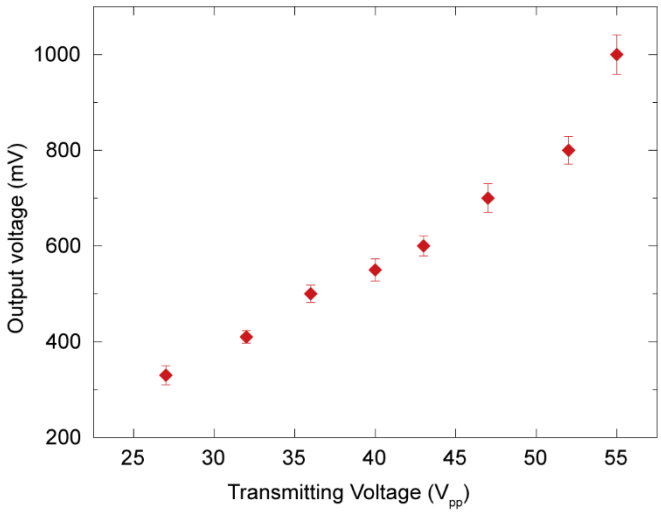


**Supplementary Fig. 22 | The output voltages generated by the sciatic nerve stimulator at a distance of 2 cm through varying transmitting voltages.**

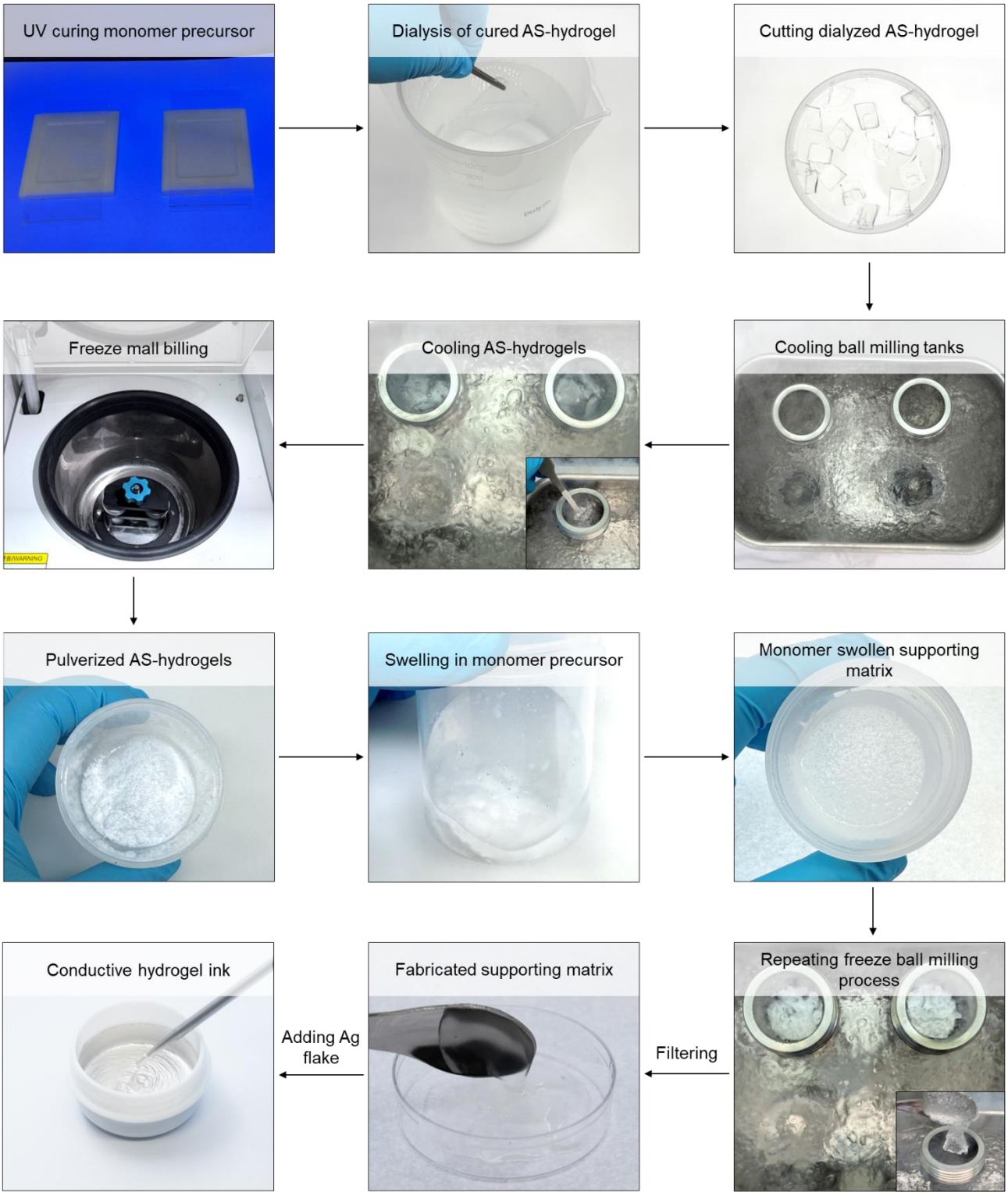


**Supplementary Fig. 23 | The fabrication process for support matrix and conductive hydrogel ink.**

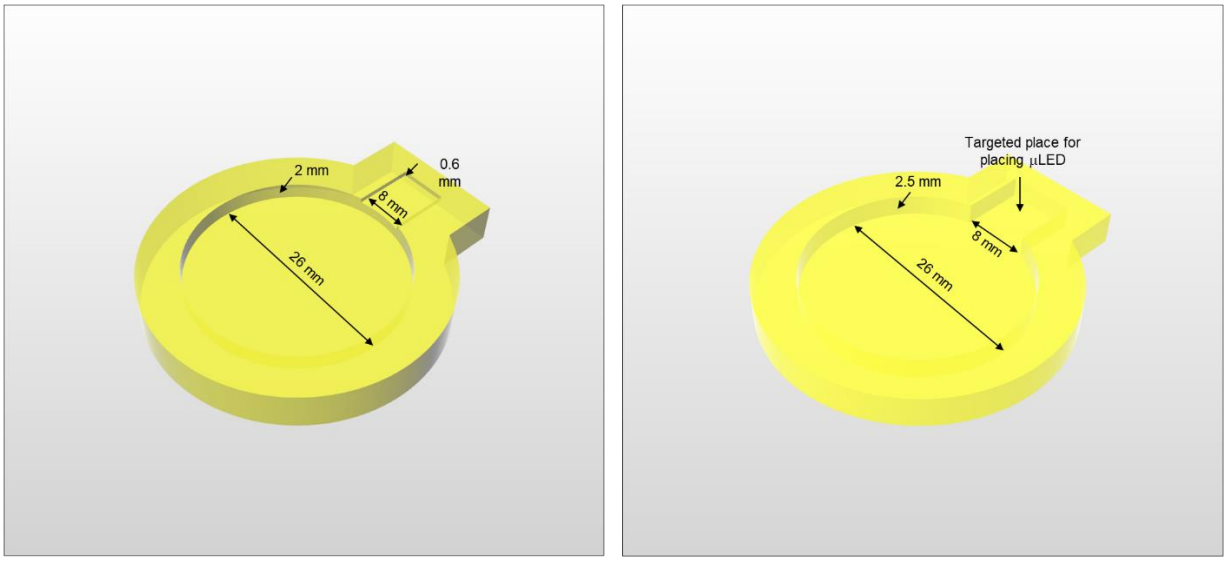


**Supplementary Fig. 24 | The printed acrylic mold for EM3DP of hydrogel inductor (a) and hydrogel optoelectronic device (b).**

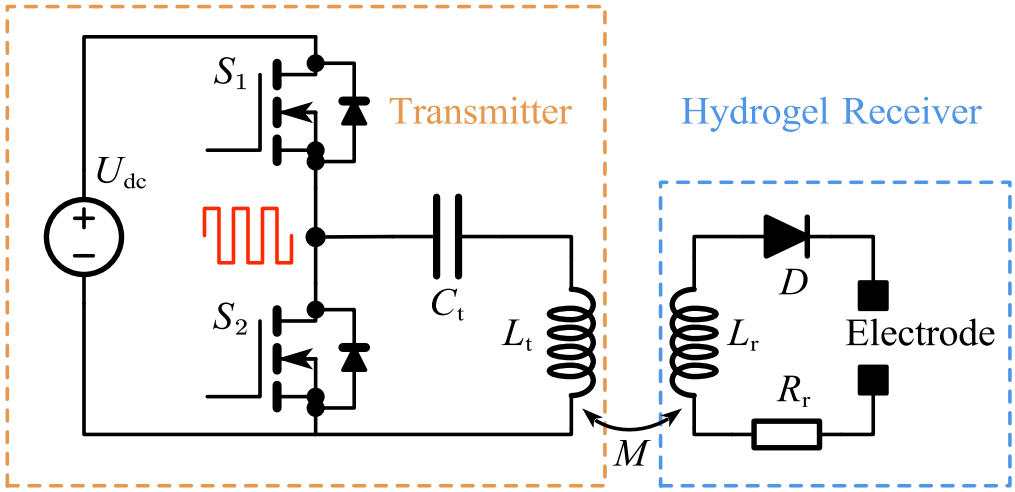


**Supplementary Fig. 25 | A circuit diagram illustrating the working mechanism of the customized wireless power transfer system and the receiving wireless-powered hydrogel bioelectronics**

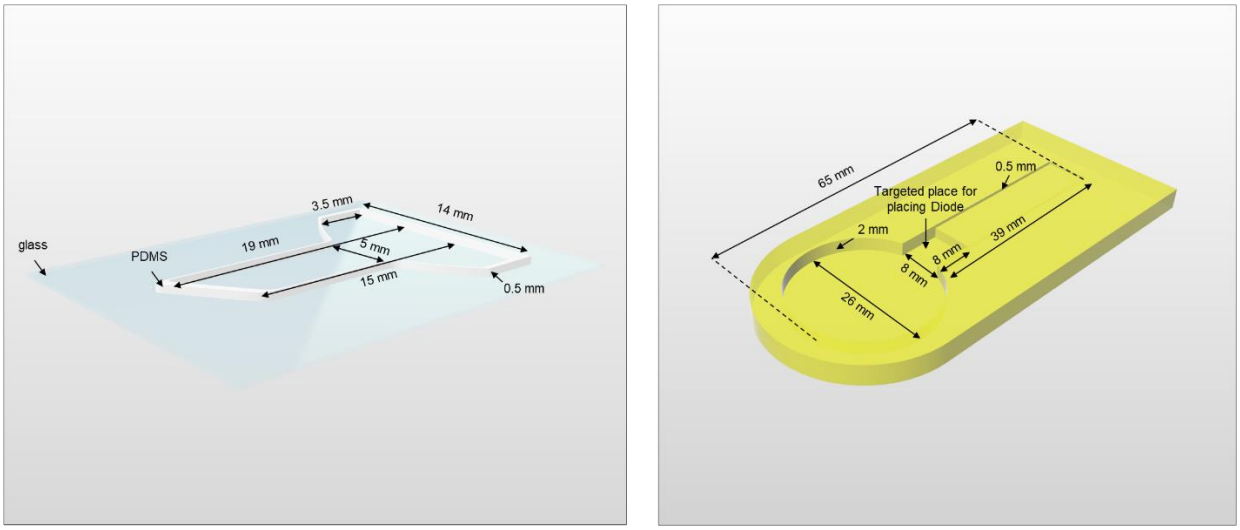


**Supplementary Fig. 26 | (a) The custom-made mold for EM3DP of all hydrogel BCIs. (b) The printed acrylic mold for EM3DP of wireless hydrogel stimulator for sciatic nerve.**

## References


1 Hui, Y. *et al.* Three-dimensional printing of soft hydrogel electronics. *Nature Electronics* **5**, 893-903 (2022).

2 Lu, B. *et al.* Pure PEDOT:PSS hydrogels. *Nature Communications* **10**, 1043 (2019).

3 Li, G. *et al.* Highly Conducting and Stretchable Double-Network Hydrogel for Soft Bioelectronics. *Advanced Materials* **34**, 2200261 (2022).

4 Won, D. *et al.* Digital selective transformation and patterning of highly conductive hydrogel bioelectronics by laser-induced phase separation. *Science Advances* **8**, eabo3209 (2022).

5 Zhou, T. *et al.* 3D printable high-performance conducting polymer hydrogel for all-hydrogel bioelectronic interfaces. *Nature Materials* **22**, 895-902 (2023).

6 Zhang, Z. *et al.* Fatigue-Resistant Conducting Polymer Hydrogels as Strain Sensor for Underwater Robotics. *Advanced Functional Materials* **33**, 2305705 (2023).

7 Sun, Z. *et al.* Strong, Tough, and Anti-Swelling Supramolecular Conductive Hydrogels for Amphibious Motion Sensors. *Small* **19**, 2303612 (2023).

8 Chong, J. *et al.* Highly conductive tissue-like hydrogel interface through template-directed assembly. *Nature Communications* **14**, 2206 (2023).

9 Li, N. *et al.* Anti-Swelling, High-Strength, Anisotropic Conductive Hydrogel with Excellent Biocompatibility for Implantable Electronic Tendon. *Advanced Functional Materials* **34**, 2309500 (2024).

10 Wang, F. *et al.* 3D Printed Implantable Hydrogel Bioelectronics for Electrophysiological Monitoring and Electrical Modulation. *Advanced Functional Materials* **n/a**, 2314471 (2024).

11 Dai, J. *et al.* Injectable Mesh-Like Conductive Hydrogel Patch for Elimination of Atrial Fibrillation. *Advanced Healthcare Materials* **13**, 2303219 (2024).

12 Won, D. *et al.* Laser-induced wet stability and adhesion of pure conducting polymer hydrogels. *Nature Electronics* **7**, 475-486 (2024).

13 Deng, J. *et al.* Electrical bioadhesive interface for bioelectronics. *Nature Materials* **20**, 229-236 (2021).

14 Tringides, C. M. *et al.* Viscoelastic surface electrode arrays to interface with viscoelastic tissues. *Nature Nanotechnology* **16**, 1019-1029 (2021).

15 Ohm, Y., Liao, J., Luo, Y., Ford, M. J. & Majidi, C. Reconfigurable Electrical Networks within a Conductive Hydrogel Composite. *Advanced Materials* **35**, 2209408 (2023).

16 Park, J. *et al.* Intrinsically Nonswellable Multifunctional Hydrogel with Dynamic Nanoconfinement Networks for Robust Tissue-Adaptable Bioelectronics. *Advanced Science* **10**, 2207237 (2023).

17 Wang, Z. *et al.* Continuous Phase Separation Induced Tough Hydrogel Fibers with Ultrahigh Conductivity for Multidimensional Soft Electronics. *Advanced Functional Materials* **n/a**, 2413478